Atmos. Chem. Phys. Discuss., https://doi.org/10.5194/acp-2019-174
Manuscript under review for journal Atmos. Chem. Phys.
Discussion started: 28 March 2019

Atmospheric Chemistry and Physics Discussions

Gas-Phase Pyrolysis Products Emitted by Prescribed Fires in Pine Forests with a Shrub Understory in the Southeastern United States**

Nicole K. Scharko[1], Ashley M. Oeck[1], Tanya L. Myers[1], Russell G. Tonkyn[1], Catherine A. Banach[1], Stephen P. Baker[2], Emily N. Lincoln[2], Joey Chong[3], Bonni M. Corcoran[3], Gloria M. Burke[3], Roger D. Ottmar[4], Joseph C. Restaino[5], David R. Weise[3], and Timothy J. Johnson[1*]

[1]Pacific Northwest National Laboratories, Richland, WA, USA
[2]USDA Forest Service, Rocky Mountain Research Station, Missoula, MT, USA
[3]USDA Forest Service, Pacific Southwest Research Station, Riverside, CA, USA
[4]USDA Forest Service, Pacific Northwest Research Station, Seattle WA, USA
[5]School of Environmental and Forest Sciences, University of Washington, Seattle WA, USA

*To whom correspondence should be addressed: Timothy.Johnson@pnnl.gov

ABSTRACT

In this study we capture and identify pyrolysis gases from prescribed burns conducted in pine forests with a shrub understory using a manual extraction device. The device selectively sampled emissions ahead of the flame front, minimizing collection of oxidized gases, with the captured gases analyzed in the laboratory using infrared absorption spectroscopy. Results show that emission ratios (ER) relative to CO for ethene, and acetylene were significantly greater than previous fire studies, suggesting that the sample device was able to collect gases prior to ignition. Further evidence that ignition had not begun was corroborated by novel infrared detections of several species, in particular naphthalene. With regards to oxygenated species, several aldehydes (acrolein, furaldehyde, acetaldehyde, formaldehyde) and the carboxylic acids (formic, acetic) were all observed; results show that ERs for acetaldehyde were noticeably greater while ERs for formaldehyde and acetic acid were lower compared to other studies. The acetylene-to-furan ratio also suggests that high temperature pyrolysis was the dominant process generating the collected gases. This hypothesis is further supported by the presence of HCN and the absence of NH_3.

Atmos. Chem. Phys. Discuss., https://doi.org/10.5194/acp-2019-174
Manuscript under review for journal Atmos. Chem. Phys.
Discussion started: 28 March 2019

Atmospheric Chemistry and Physics Discussions

1. INTRODUCTION

Biomass burning contributes large quantities of trace gases into the earth's atmosphere (Crutzen and Andreae, 1990; Akagi et al., 2011; Andreae and Merlet, 2001; Crutzen et al., 1979; Yokelson et al., 2013; Andreae, 1991). The primary carbon-containing gases emitted during such burns are CO_2, CO and CH_4, in order of decreasing concentration (Ward and Hardy, 1991). Hundreds of other trace gases have also been identified in the emissions, including many non-methane volatile organic compounds (NMVOCs), oxygenated volatile organic compounds (OVOCs), nitrogen-containing species and sulfur compounds (Yokelson et al., 1996; Lobert et al., 1991; Talbot et al., 1988). The major sources of biomass burn emissions are wildland fire and, to a lesser extent, prescribed fire. Prescribed fires are used by foresters, other officials and private land owners to reduce dangerous fuel buildups and manage habitats (Fernandes and Botelho, 2003). The use of prescribed fire as a preventative tool is of particular importance in the western United States (U.S.) where wildland fires are increasing in severity (Turetsky et al., 2011; Miller et al., 2009). In the southeastern U.S., prescribed fire is also used on a routine basis for purposes such as ecosystem management (Waldrop and Goodrick, 2012). For these and other beneficial reasons, an estimated 3.6 million hectares of forestry land have been burned in the U.S. by prescribed fire each year (Melvin, 2012). Agencies that conduct such burns often rely on fire-related models (Reinhardt et al., 1997; Prichard et al., 2006) to predict the impacts of the prescribed burn. Having detailed knowledge of the emission products can thus improve the predictive output of such regional models (Reid et al., 2009).

Due to the influential role of wildland fire on atmospheric chemistry and climate, there has been considerable interest in identifying and quantifying gas emissions from fire as studied both in the

54 laboratory and in field burns (Crutzen et al., 1979; Andreae et al., 1988; Lobert et al., 1991;
55 Andreae et al., 1994; Lindesay et al., 1996; Goode et al., 1999; Yokelson et al., 1999; Yokelson et
56 al., 1996; Chi et al., 1979). The type of gases emitted and their relative abundances depend on
57 many factors such as fuel type, fuel arrangement, land management activities, burning techniques
58 and environmental conditions (Ward et al., 1996; Ward et al., 1992). In the 1990s, Griffith,
59 Yokelson and co-workers conducted a series of laboratory studies using an open-path Fourier
60 transform infrared (FTIR) spectrometer to investigate how some of these factors influence the
61 emitted gases (Goode et al., 1999; Yokelson et al., 1996; Yokelson et al., 1997). There have been
62 several follow-on laboratory studies using IR spectroscopy along with other analytical techniques
63 to identify previously unknown fire emission products and to derive emission factors from various
64 fuel types (Burling et al., 2010; Hatch et al., 2017; Selimovic et al., 2018; Stockwell et al., 2014;
65 Yokelson et al., 2013; Gilman et al., 2015).
66
67 In addition to the laboratory studies, a number of field campaigns have also used FTIR
68 spectroscopy to identify trace gases from prescribed fires (Akagi et al., 2013; Burling et al., 2011;
69 Akagi et al., 2014; Goode et al., 2000; Yokelson et al., 1999; Wooster et al., 2011; Alves et al.,
70 2010; Hurst et al., 1994a; Hurst et al., 1994b; Paton-Walsh et al., 2010; Paton-Walsh et al., 2008;
71 Guérette et al., 2018). Studies that have the ability to measure emissions both near the fire and
72 aloft are especially useful in understanding the complex chemistries that occur during and after
73 prescribed fires, including the (oxidative) chemistry of the downwind plume. For example, (Akagi
74 et al., 2013) detected limonene from a prescribed burn with a land-based FTIR and linked it to the
75 production of ozone, formaldehyde and methanol, all of which were measured downwind with an
76 airborne-based FTIR. In an earlier prescribed burn study, Burling et al. (2011) detected enhanced

77 levels of isoprene and 1,3-butadiene in the smoke from a living tree when compared to dead stumps
78 under the same conditions. Emission characteristics obtained during such campaigns can be
79 especially useful for the implementation or verification of effective burning techniques to
80 minimize the gases released during prescribed burns.
81
82 However, few investigations have studied the pre-ignition or pyrolysis gases emitted prior to the
83 flaming combustion stage. Most prescribed burn studies have focused only on the flaming and
84 smoldering stages. The hotter flaming stage is characterized by more oxidized products and a
85 higher modified combustion efficiency (MCE) (Ward and Hao, 1991), which is defined as:

$$\mathrm{MCE} = \left(\frac{\Delta CO_2}{\Delta CO_2 + \Delta CO}\right). \quad (1)$$

86 The cooler smoldering phase with lower MCE values (typically ranging from 0.65–0.85)
87 (Urbanski, 2013) displays more non-oxidized or less-oxidized species. The present study differs
88 from these earlier works in that we exclusively attempt to investigate pyrolysis, which is the first
89 step in the burning process (Collard et al., 2014), in particular we investigate the gas phase
90 pyrolysis species generated during prescribed burns. Primary mechanisms associated with
91 pyrolysis of biomass are char formation, depolymerization and species fragmentation. Volatile
92 products are generated and, if unstable, can continue to undergo secondary (non-combustion)
93 reactions such as cracking or recombination (Collard and Blin, 2014). Pyrolytic reactions produce
94 fuel gases that, if sufficient in quantity and in the presence of oxygen, will maintain the flame via
95 combustion pathways (Ward and Hardy, 1991; Di Blasi, 1993). Thus, the primary objectives of
96 the present study are a) to detect pyrolysis gases in prescribed burns (i.e. gases that are emitted
97 prior to the flame front and prior to the onset of combustion) and b) to determine if they are
98 different from pyrolysis gases measured under more tightly controlled laboratory conditions.

99

100 There have been several pyrolysis laboratory studies carried out in controlled environments: In
101 one of the earliest investigations, DeGroot et al. (1988) detected H_2O, CO_2, CH_3OH, HCOOH and
102 CH_3COOH from the pyrolysis of wood. More recent studies have observed several other
103 compounds, such as CO, CH_4, light weight hydrocarbons (C_2–C_5) and light tar compounds (e.g.
104 benzene and its derivatives and polycyclic aromatic hydrocarbons) from the slow pyrolysis of
105 Birch wood (Fagernäs et al., 2012). Oxygenated compounds (e.g. furan-related compounds) have
106 been observed from the fast pyrolysis of levoglucosan, a known pyrolyzate of cellulose (Bai et al.,
107 2013). Laboratory experiments that have investigated condensed and/or gas phase compounds
108 generated by pyrolysis under controlled conditions have revealed that the speciation and
109 distribution of the products are dependent on a number of factors such as heating rate, temperature,
110 fuel composition, live vs. dead fuels and amount of available oxygen (Azeez et al., 2011; Lu et al.,
111 2011; Shen et al., 2010; Safdari et al., 2018; Ren and Zhao, 2012, 2013a, b). For instance, Ren and
112 coworkers (2013a) found that the amount and speciation of nitrogen containing pyrolyzates is
113 complicated and influenced by the content of mineral matter, the presence of oxygen (Ren and
114 Zhao, 2012), as well as the structure (e.g. aliphatic vs. heterocyclic) of the amino acids and the
115 amount of cellulose, hemicellulose and lignin in the sample. Similarly, the release of oxygenated
116 compounds (e.g. phenolic compounds) from the pyrolysis of lignin is sensitive to the presence of
117 oxygen (Kibet et al., 2012). The pyrolysis studies mentioned above were conducted in controlled
118 settings or on smaller scales. There remains a paucity of data that identify and quantify gas-phase
119 pyrolysis species emitted from actual prescribed burns at the field scale.

120

To our knowledge, this is one of the first field studies that discriminatively measures pyrolysis gases for southeastern U.S. fuels. Isolating such species is indeed challenging as they often blend with the background atmosphere and are rapidly mixed with other gases at the onset of combustion. One must thus isolate the "pyrolysis molecules" either optically, mechanically or temporally. In this study, we selectively probe the pyrolysis gases by using a simple manually-operated spatial collection device that attempts to ensure that only gases in front of the flame are collected. While not a perfect solution, the information gathered in this study adds important insights into the primary products generated during the pyrolysis process.

2. EXPERIMENTAL

2.1 Site description

During the week of 29 April 2018, a total of seven small plots (160 m^2) were burned using prescribed fire at Ft. Jackson, South Carolina (SC), latitude: 34.05 and longitude: –80.83, approximately 10 km east of Columbia, SC. The fort lies entirely within the Sandhills ecosystem in the South Carolina coastal plain, which runs approximately parallel to the Atlantic Ocean coast, 175 km inland. The Sandhills region thus forms a belt that tracks southwest – northeast across sands of varying depth with a high content of pure silica (Porcher and Rayner, 2001). The deep sands support an overstory vegetation that has significant amounts of turkey oak (*Quercus laevis* Walter) and two native pine species relatively unique to the southeastern U.S.: longleaf pine (*Pinus palustris* Mill.) and slash pine (*Pinus elliottii* Engelm.). The understory has substantial quantities of immature turkey oak, longleaf and slash pine, along with sparkleberry (*Vaccinium arboreum* Marshall) and a heterogeneous organic layer of woody material, litter, duff and cones atop the mineral soil. The longleaf ecosystem depends on fire for maintenance (Cary, 1932). Site details

Atmos. Chem. Phys. Discuss., https://doi.org/10.5194/acp-2019-174
Manuscript under review for journal Atmos. Chem. Phys.
Discussion started: 28 March 2019

Atmospheric Chemistry and Physics Discussions

144 for the seven burn plots, all with a 2 year rough (i.e. burned 2 years prior), are summarized in Table
145 1. Eight pre- and post-fire 1.0 meter square biomass clipped plots were established at each 160 m^2
146 research block where organic vegetative material in each site was collected before and after each
147 fire. Shrub, grasses/forbs, down woody material (0-0.6, 0.6-2.5, 2.5-7.6 7.6-22.9 cm in diameter),
148 litter and duff, are the major fuel bed components that were targeted. Fuel moisture samples for
149 each major component were collected before ignition to determine fuel moisture content for each
150 fuel bed component. Figure 1 shows photographs of site 16, plot 1 before, during and after the
151 burn as well as a thermal image of the flame interacting with the fuel.
152

Atmos. Chem. Phys. Discuss., https://doi.org/10.5194/acp-2019-174
Manuscript under review for journal Atmos. Chem. Phys.
Discussion started: 28 March 2019

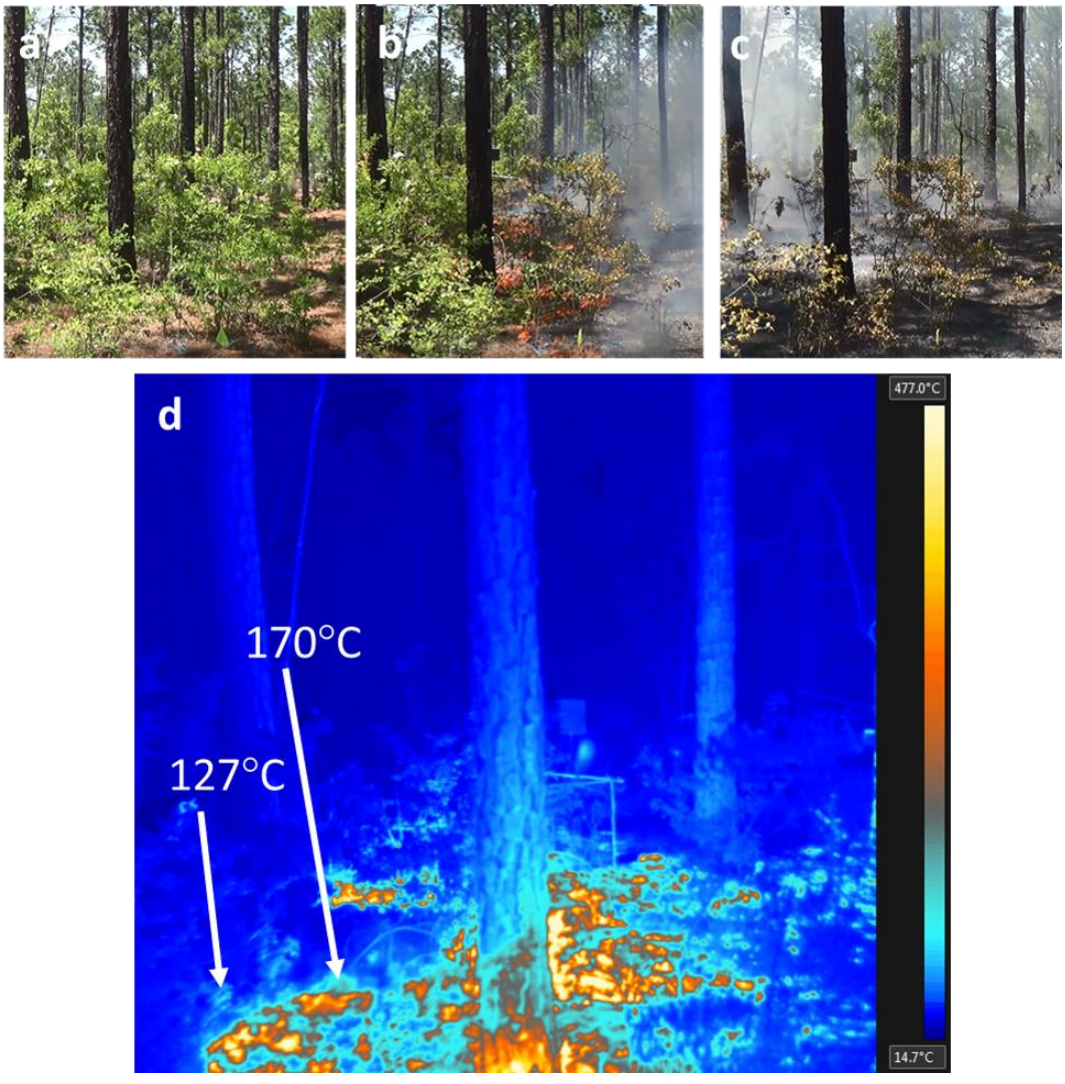

Figure 1. Photographs of site 16, plot 1 on 3 May 2018 between 14:00 and 14:40 local time. The plot (a) before the flame, (b) while the flame interacted with the fuel at 14:33 and (c) smoldering combustion of the fuel. The primary species seen in the understory are sparkleberry and a litter layer of pine needles. (d) Thermal image of the flame interacting with the fuel at time of 14:33.

Atmos. Chem. Phys. Discuss., https://doi.org/10.5194/acp-2019-174
Manuscript under review for journal Atmos. Chem. Phys.
Discussion started: 28 March 2019

Atmospheric Chemistry and Physics Discussions

Table 1. Plot name, date/time, fuel description, atmospheric conditions (all clear sky days) and plot mixing height and area for the prescribed burns.

Burn plot	Date (2018)	Local start time (EDT)	Local finish time (EDT)	Dominant overstory	Understory fuels	Ambient temperature (°C)	Relative humidity (%)	Surface winds (m s^{-1}) and wind direction	Mixing height (m)	Area burned (m^2)
24B-triangle	1-May	12:11	12:37	slash pine	sparkleberry/ logs	24	26	2.7 SW	975	450
24B-north diamond	1-May	13:53	14:43	slash pine	sparkleberry/ logs	28	18	2.7 SW	1310	900
24A-square	2-May	9:37	10:22	longleaf pine	sparkleberry/ duff	21	53	2.7 SW	792	900
24A-triangle	2-May	12:08	12:43	longleaf pine	sparkleberry/ duff	27	34	2.7 SW	1189	450
16 plot 5	3-May	9:39	10:21	longleaf pine	sparkleberry/ bracken fern	22	59	2.7 SW	579	900
16 plot 6	3-May	11:44	12:13	longleaf pine	sparkleberry/ turkey oak	26	43	3.1 SW	1067	900
16 plot 1	3-May	13:56	14:41	longleaf pine	sparkleberry/ turkey oak	29	30	3.1 SW	1494	900

2.2 Collection device

Our approach to sampling used an extractive collection device whose tube inlet sampled air and emissions directly ahead of the flame. This simple solution is similar to other canister methods often used with gas chromatographic analysis (Young et al., 1997) and also conceptually similar to the land-based FTIR used to sample emissions as described by Akagi et al. (2013, 2014) and Burling et al. (2011). The canister sampling package, mounted on a metal frame, contained a set of evacuated canisters which were carried to the individual burn plots. The sampling package consisted of a 12-Volt Swing Piston KNF Neuberger Pump (NPK09DC) plumbed with stainless steel tubing to a pressure relief valve and gauge. The pressure relief valve was adjustable to regulate the pressure of the system and ultimately the fill pressure of the canisters. The flow rate to fill the canisters was 15 liters min^{-1}. A sampling probe (2.5 m of 6 mm stainless steel tubing plus 2 m of flexible stainless-steel line) was attached to the inlet of the package to collect pyrolysis gases from point sources of vegetation within the burning plots (Figure S1 displays a photo of the device). The device had an in-line two-way valve to control the sampling interval. To capture a

pyrolysis sample, the probe was placed near the base of the flame, immediately above the fuel where the pyrolysis gases should be emitted at maximal levels. Seven to ten aliquots of gas sample were added to a single canister as the device was moved in front of the flame to capture pyrolysis gases. Each 3-liter Summa canister was filled to approximately 138 kPa (20 psia) for the FTIR analysis.

2.3 FTIR Spectrometer and Spectral Analysis

The experimental details regarding FTIR measurement procedures have been previously reported (Scharko et al., 2018). The FTIR spectrometer parameters and measurement details are briefly summarized as is the spectral analysis: Gases in the canisters were returned from the field to the laboratory and analyzed the same day or the following day using an 8 meter White cell (Bruker Optics, A136/2-L) and FTIR; canisters were connected to the gas cell via 3/8" stainless steel tubing with both the tubing and gas cell heated to 70 °C to prevent analyte adhesion. The cell was coupled to a purged FTIR (Bruker Optics, Tensor 37) spectrometer equipped with a glow bar source, KBr beamsplitter and liquid nitrogen cooled mercury cadmium telluride (MCT) detector. Spectra were collected from 4000 to 500 cm^{-1} at 0.6 cm^{-1} resolution.

Spectral analysis was carried out using the MALT5 program (Griffith, 2016) and 50 °C reference spectra from the PNNL database (Sharpe et al., 2004; Johnson et al., 2010) as well as absorption lines from HITRAN (Gordon et al., 2017). MALT5 fits the assigned reference spectral lines to the measured spectrum by optimizing the fit of all gases ascribed to the spectral window and minimizing the residual. The calculation involves input parameters such as path length, resolution and apodization accompanied by reference absorption cross-sections and the measured spectrum

Atmos. Chem. Phys. Discuss., https://doi.org/10.5194/acp-2019-174
Manuscript under review for journal Atmos. Chem. Phys.
Discussion started: 28 March 2019

with its associated temperature and pressure values. Both H_2O and CO_2 had peaks that were optically saturated; these regions were eliminated from analysis (Table S1 displays the analytes of interest and the spectral region used for the fit). In some instances, peaks for the gases of interest were also saturated in which case the pressure in the gas cell was reduced and the measurement repeated.

2.4 Calculation of emission ratios and emission factors

A convenient quantity to compare emissions between burns is the emission ratio (ER). This ratio is calculated by the change in the analyte of interest relative to the change in some known gas, typically CO or CO_2. For the present study, the change in analyte is divided by the change in CO:

$$ER = \left(\frac{\Delta analyte}{\Delta CO}\right). \quad (2)$$

It is important to note that these are the changes in analyte and CO relative to background atmosphere (i.e. relative to ambient "clean air" conditions). The background levels of CO and CO_2 were measured using an open path gas analyzer (OPAG 22) prior to the series of burns. The initial CO_2 level was measured to be 409 ppm (this value agrees with the global averaged CO_2 for May 2018 of 408.7 ppm (Dlugokencky and Tans)) whereas the CO level was often below the OPAG detection limit. Without an instrument to measure ambient CO with sufficient sensitivity we arbitrarily chose 200 ppb for an estimated background level which is within the range for a typical CO mixing ratio (Seinfeld and Pandis, 2012). Emission ratios can be calculated for a single point in time during the fire or they can incorporate the full length of the fire. The present ERs were calculated based on the contents of the individual canisters and represent discrete ERs. Other studies have obtained fire-integrated ERs, which integrate over the entire duration of the fire (Koss

Atmos. Chem. Phys. Discuss., https://doi.org/10.5194/acp-2019-174
Manuscript under review for journal Atmos. Chem. Phys.
Discussion started: 28 March 2019

Atmospheric Chemistry and Physics Discussions

et al., 2018) or fire-averaged ERs determined from the slope of the regression with the intercept set to zero (Yokelson et al., 1999).

Another useful quantity is the emission factor (EF), defined as the number of grams emitted of a given analyte per kilogram of dry fuel consumed and estimated using the following equation (Yokelson et al., 1999):

$$EF\ (g\ kg^{-1}) = F_{carbon} \times 1000 \times \frac{MW_{analyte}}{MW_{carbon}} \times \frac{\frac{\Delta analyte}{\Delta CO_2}}{\sum_{j=1}^{n}\left(NC_j \times \frac{\Delta C_j}{\Delta CO_2}\right)} \quad (3)$$

where F_{carbon} is the mass fraction of carbon in the fuel, $MW_{analyte}$ and MW_{carbon} are the molar masses of the analyte and carbon, respectively, $\frac{\Delta analyte}{\Delta CO_2}$ is the emission ratio of the analyte relative to CO_2, $\frac{\Delta C_j}{\Delta CO_2}$ is the emission ratio of species *j* relative to CO_2 and NC_j is the number of carbons in species *j*. Note that ΔCO_2 cancels out in equation 3. Elemental analysis of similar southeastern fuels was reported in a previous study (Safdari et al., 2018), and the average carbon content by mass for longleaf pine foliage and litter as well as sparkleberry was 0.52 which was used for F_{carbon}. (Table S2 displays the elemental analysis for each fuel from Safdari et al., 2018). One assumption in equation 3 is that all of the carbon in the fuel is released and accounted for in the measurements of the *j* carbon species. Most carbon emissions are in the form of CO_2, CO or CH_4. It should be noted that the EF quantities reported here include only compounds measured by the FTIR, and EF values may be overestimated by 1 to 2% due to undetected carbon species (Akagi et al., 2011).

2.5 OH Reactvity

Wildland fires release gases that may react with the hydroxyl radical (OH) to impact secondary formation of ozone and downwind aerosols. To gauge the atmospheric chemistry effects of the total gases emitted during the burns, the total OH reactivity (in units of s^{-1} ppm CO^{-1}) for each of the plots was determined by summing all of the ERs for each reactive gas multiplied by its corresponding second order OH rate constant (k_{OH} in units of cm^3 $molecules^{-1}$ s^{-1}) and a conversion factor as outlined by Gilman et al. (2015). The conversion factor used for the present calculations was 2.46×10^{13} molecules cm^{-3} ppm^{-1}. The rate constants were obtained from the NASA Panel for Data Evaluation (Sander et al., 2006), Gilman et al. (2015), Atkinson et al. (2000) and the NIST Chemical Kinetics Database.

3. RESULTS AND DISCUSSION

3.1 Estimating the contribution from high and low temperature processes

In a recent study Sekimoto et al. (2018) suggested that MCE may not be the best quantity to adequately describe pyrolysis, but rather that emissions of volatile organic compounds (VOCs) from biomass burning may be correlated with high and low temperature pyrolysis factors obtained by carrying out positive matrix factorization (PMF) analysis on the emission profiles. The authors further suggested that the ratio of acetylene (C_2H_2) to furan (C_4H_4O) could be used to estimate the high and low temperature pyrolysis factors. They used the emission profiles from the analysis of 15 different fuels to calculate the following ratio that estimates the high and low temperature VOC emissions:

$$\frac{(\text{Total VOC})_{\text{High T}}}{(\text{Total VOC})_{\text{Low T}}} = \frac{C_2H_2 \,/\, 0.0393}{C_4H_4O \,/\, 0.0159}. \quad (4)$$

Atmos. Chem. Phys. Discuss., https://doi.org/10.5194/acp-2019-174
Manuscript under review for journal Atmos. Chem. Phys.
Discussion started: 28 March 2019

Atmospheric Chemistry and Physics Discussions

We adopted this estimation approach and have used the acetylene to furan ratio to assess the relative contributions from high and low temperature processes. The average results are displayed in Figure 2 alongside the results from Koss et al. (2018), Gilman et al. (2015) and Akagi et al. (2013). For comparison purposes, the values displayed in Figure 2 were determined using average ERs for acetylene and furan. The present results are approximately an order of magnitude greater than all previous studies, likely due to the timing of collection and the sampling probe's proximity to the flame. The juxtaposed values from the previous studies were obtained using either a) fire-integrated ERs, b) discrete ERs sampled every 20 to 300 sec or c) fire-averaged ERs, all of which incorporate several different phases of the fire as compared to the present measurements which represent discrete samples just seconds before the flame front. With the Sekimoto et al. estimation approach, higher acetylene/furan ratios indicate a greater contribution from the high temperature process. The markedly high ratio observed in this study suggests that samples were collected when high temperature pyrolysis was indeed the dominant process. This observation is consistent with the time profile for the contribution of the high temperature pyrolysis factor presented by Sekimoto et al. (2018), which demonstrates that the contribution from high temperature pyrolysis [High-T / (High-T + Low-T)] can easily exceed 0.95 in the early stages of fire, but reduces to smaller fractions (≤ 0.3) in the latter stages. Another key difference is that the sampling probe used at Ft. Jackson was positioned so as to extract gases directly before the flame front, yet in close proximity to it, in order to limit further reactions. In particular, if the highly flammable acetylene molecules were captured prior to subsequent oxidation reactions, this would explain the enhanced ratio of high to low temperature VOC emissions as seen in Figure 2.

Atmos. Chem. Phys. Discuss., https://doi.org/10.5194/acp-2019-174
Manuscript under review for journal Atmos. Chem. Phys.
Discussion started: 28 March 2019

Atmospheric Chemistry and Physics Discussions

289

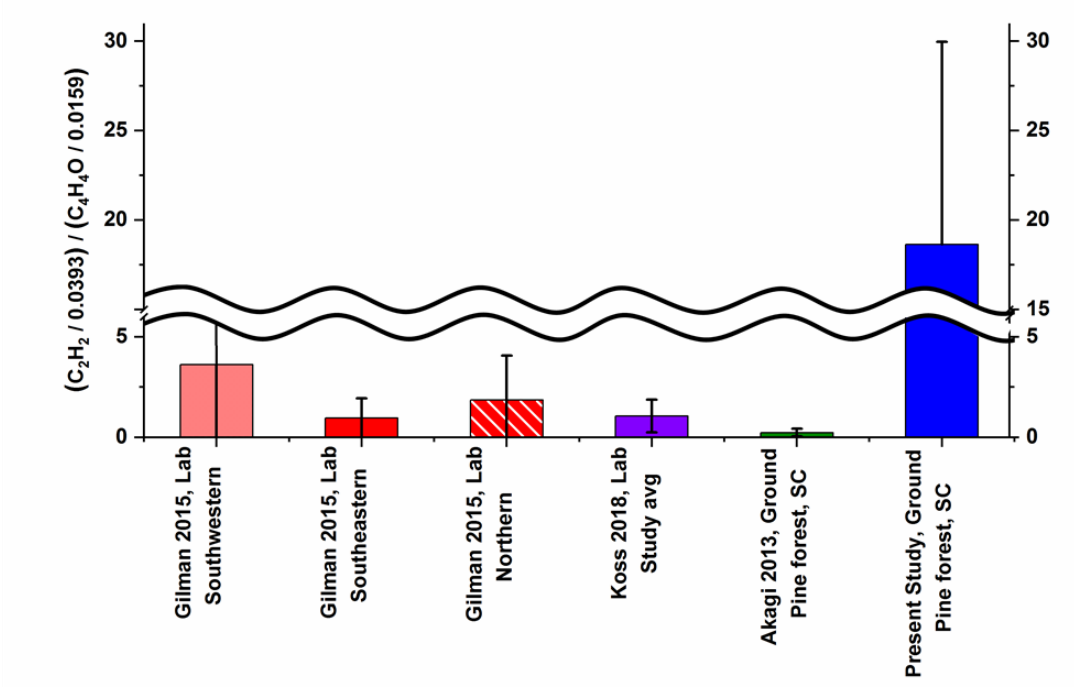

290

291 **Figure 2.** Ratio of acetylene (C_2H_2)/0.0393 to furan (C_4H_4O)/0.0159 to predict the ratio of high to low temperature
292 VOC emissions as outlined by Sekimoto et al. (2018). Error bars represent 1σ. For the present study average results
293 were determined from the 10 collected samples preceding the flame front for acetylene and furan. Koss et al. (2018)
294 values were fire integrated while Gilman et al. (2015) used 20-300 sec integrations. Akagi et al. (2013) reported EFs
295 which were used to calculate ERs for acetylene and furan.

Atmos. Chem. Phys. Discuss., https://doi.org/10.5194/acp-2019-174
Manuscript under review for journal Atmos. Chem. Phys.
Discussion started: 28 March 2019

296 ### 3.2 CO_2 and CO Emissions and MCE Values

297 As expected, other than H_2O vapor, CO and CO_2 were the predominant gases observed as
298 emissions. Table 2 displays the EF (g kg^{-1}) and ER (ppb/ppm_{CO}) values averaged for the ten field
299 measurements, while Tables S3 and S4 contain the individual values for each measurement. The
300 average MCE for all ten measurements was 0.83 ± 0.04, ranging from 0.75 to 0.87. Such MCE
301 values would normally characterize data gathered during smoldering combustion where a
302 combination of processes such as pyrolysis along with glowing combustion of char take place
303 (Yokelson et al., 1997). Higher MCE values are associated with the flaming stage (~0.99 for pure
304 flaming) and indicate more efficient combustion (i.e. a higher reaction temperature and more
305 complete oxidation of the organic matter, while lower values (~0.65-0.85) are associated with the
306 smoldering stage (Urbanski, 2013). Since the present study aimed at collection of pyrolysis gases
307 preceding the flame front, characterizing the results in terms of MCE values may not be
308 appropriate: The lower MCE values do not represent the fire being in the smoldering stage, but
309 rather suggest that pyrolysis products were captured (at least in part) prior to the onset of
310 combustion. As noted, the methodology used with this collection device ideally extracted the
311 pyrolysis gases before they combusted. Due to the proximity of these gases to the flame and the
312 surrounding atmosphere, however, air and combustion products in the region of sampling were
313 likely captured along with pyrolysis gases.

314

315

Atmos. Chem. Phys. Discuss., https://doi.org/10.5194/acp-2019-174
Manuscript under review for journal Atmos. Chem. Phys.
Discussion started: 28 March 2019

Atmospheric Chemistry and Physics Discussions

316 **Table 2.** Study averages of MCE Study (0.83 ± 0.04), EF (g kg–1) and ER (ppb/ppm$_{CO}$) for
317 the ten measurements along with standard deviation (SD). SD represent the variation for the
318 ten non-identical measurements.

Species	Formula	EF Study Average (g kg^{-1})	SD	ER Study Average (ppb/ppm$_{CO}$)	SD
Carbon dioxide	CO_2	1469	113	5190	1450
Carbon monoxide	CO	191	45	1000	n/a
Methane	CH_4	11.2	3.9	101.3	18.7
Ethane	C_2H_6	1.14	0.42	5.54	1.48
Ethene	C_2H_4	11.8	3.8	61.1	9.6
Acetylene	C_2H_2	7.4	3.1	40.9	10.4
Propene	C_3H_6	2.69	1.04	9.32	2.34
Allene	C_3H_4	0.30	0.12	1.09	0.23
1,3-Butadiene	C_4H_6	1.20	0.72	3.13	1.25
Isobutene	C_4H_8	0.23	0.15	0.58	0.31
Isoprene	C_5H_8	0.63	0.90	1.18	1.43
Naphthalene	$C_{10}H_8$	0.65	0.36	0.77	0.47
Formaldehyde	HCHO	0.76	0.98	3.63	4.57
Methanol	CH_3OH	1.39	1.40	6.11	5.56
Formic acid	HCOOH	0.23	0.14	0.74	0.42
Acetaldehyde	CH_3CHO	2.84	1.41	9.35	3.59
Acetone	$(CH_3)_2CO$	1.15	0.77	2.92	1.78
Acetic acid	CH_3COOH	1.45	2.66	3.46	6.15
Acrolein	C_3H_4O	1.59	1.01	4.10	2.15
Furan	C_4H_4O	0.41	0.25	0.89	0.49
Furaldehyde	C_4H_3OCHO	1.01	1.01	1.45	1.31
Hydrogen cyanide	HCN	1.34	0.31	7.34	1.25
Nitrous acid	HONO	0.10	0.16	0.30	0.46
Methyl nitrite	CH_3ONO	0.41	0.32	1.06	0.90

319
320

321

322

323 ### 3.3 Emissions of Lightweight Hydrocarbons

Besides CO and CO_2, the second most abundant class of gases generated during the prescribed burns was lightweight hydrocarbons (HCs). The lightweight HCs detected by the FTIR include methane, ethane, ethene, acetylene, propene, allene, 1,3-butadiene, isoprene and isobutene. Most of these (except allene) have been previously identified in fire emissions using FTIR either in laboratory experiments (Burling et al., 2010; Christian et al., 2003; Christian et al., 2004; Gilman et al., 2015; Goode et al., 1999; Hatch et al., 2017; Selimovic et al., 2018; Stockwell et al., 2014; Yokelson et al., 1996; Yokelson et al., 1997) or field settings (Akagi et al., 2013; Akagi et al., 2014; Alves et al., 2010; Burling et al., 2011; Goode et al., 2000; Hurst et al., 1994a; Hurst et al., 1994b; Karl et al., 2007; Paton-Walsh et al., 2010). Figure 3 shows the individual correlations between these lightweight HCs and excess CO mixing ratios. The analyte vs. ΔCO correlation coefficients range from 0.97 (ethene and allene) to 0.66 (isoprene and isobutene). In all cases, the correlation coefficients were larger with CO than with CO_2. Positive relationships have been observed for CO correlations in previous burning studies (Hurst et al., 1994a; Hurst et al., 1994b).

Atmos. Chem. Phys. Discuss., https://doi.org/10.5194/acp-2019-174
Manuscript under review for journal Atmos. Chem. Phys.
Discussion started: 28 March 2019

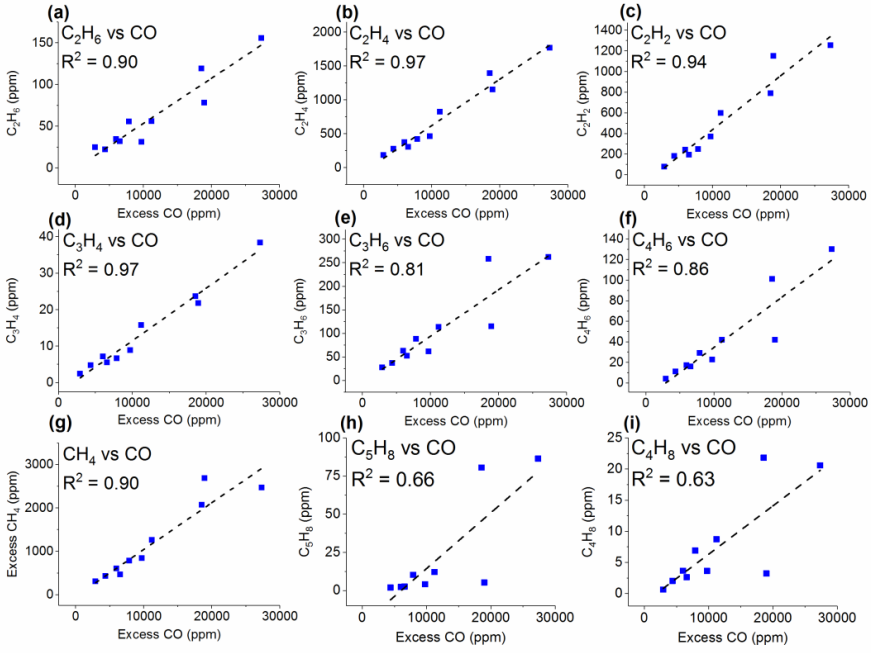

Figure 3. Mixing ratios (ppm) for the 10 measurements as a function of excess CO (ppm) for (a) ethane (C_2H_6), (b) ethene (C_2H_4), (c) acetylene (C_2H_2), (d) allene (C_3H_4), (e) propene (C_3H_6), (f) 1,3-butadiene (C_4H_6), (g) excess methane (CH_4), (h) isoprene (C_5H_8) and (i) isobutene (C_4H_8). The dashed lines are a linear fit to the data.

While the observed emission ratio (ER) for excess methane was comparable, ERs for ethene and acetylene were considerably greater than previously reported values; specifically, Figure 4 shows a comparison for methane, ethene and acetylene to previously reported values of Gilman et al. (2015) and Akagi et al. (2013). As noted, different sampling methods complicate the comparison. The present data represent a collection of instantaneous grab samples extracted directly before the flame front, whereas the other data represent time averaged values. Ethene and acetylene have both been observed as pyrolysis products in prior laboratory work (Palma, 2013), but may react further. For example, the addition reaction of acetylene to benzene or naphthalene can produce styrene or cyclopenta-fused polycyclic aromatic hydrocarbons (PAHs) (Ledesma et al., 2002). Alternatively

Atmos. Chem. Phys. Discuss., https://doi.org/10.5194/acp-2019-174
Manuscript under review for journal Atmos. Chem. Phys.
Discussion started: 28 March 2019

ethene and acetylene can undergo combustion (Simmie, 2003). Nevertheless, the high ER values for ethene and especially for acetylene in the present study further suggest that the samples were collected when the high temperature pyrolysis process was dominant; Sekimoto et al. (2018) also observed that high temperature pyrolysis profiles are often associated with aliphatic unsaturated hydrocarbons.

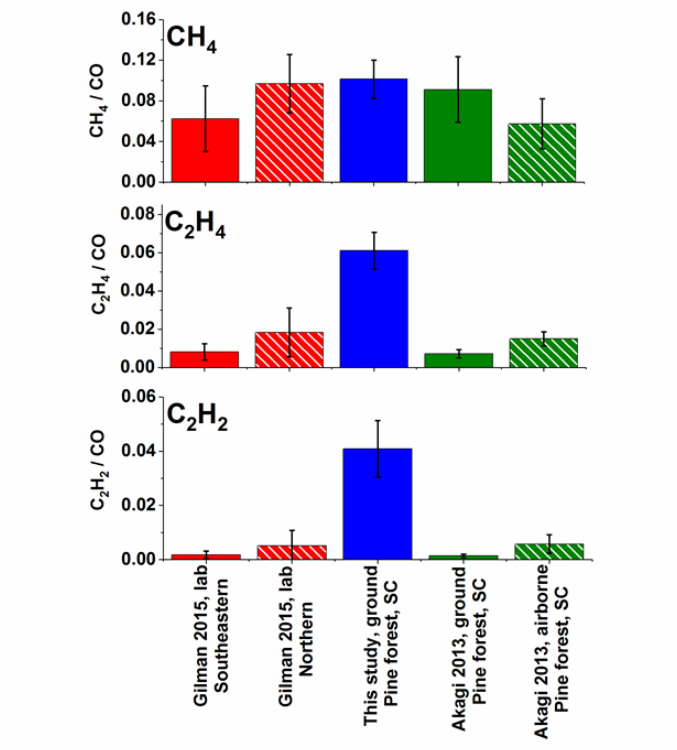

Figure 4. Average emission ratios (ppm/ppm$_{CO}$) for excess methane (top), ethene (middle) and acetylene (bottom) for this study and for previously published laboratory and field (ground and air based) investigations. Error bars represent 1σ. Gilman et al. (2015) present discrete ERs with sample acquisition of 20 to 300 sec. Akagi et al. (2013) present fire-averaged EFs calculated using ERs derived by the regression method. The emission ratios for Akagi et al. shown above were derived from the ratio of the emission factors for the gas of interest and CO multiplied by the molar mass of CO/molar mass of analyte.

3.4 Emissions of Lightweight Oxygenated Hydrocarbons

The noncyclic oxygenated hydrocarbons detected via FTIR analysis include formaldehyde, methanol, formic acid, acetaldehyde, acetone, acetic acid and acrolein. Figure 5 shows average

ERs for these species along with the cyclic compounds furan and furaldehyde. On average, acetaldehyde and methanol had the highest ER values in this group, with ER relative to CO of 0.009 and 0.006, respectively. Individual ERs per burn plot are displayed in Figure S2. Figure S2a presents the results from site 16, while Figure S2b contains results from sites 24A and 24B. For all measurements collected at sites 16 and 24A, acetaldehyde was consistently the highest with ER values ranging from 0.005 to 0.014. Site 24B followed a different trend with highest ER values for acetic acid, methanol, acetaldehyde and formaldehyde (in decreasing order). The ERs for acetic acid and formaldehyde at site 24B are at least 7.9 and 2.5 times greater, respectively, than the other burn sites: One key difference for site 24B was fuel composition, namely the presence and partial consumption of larger logs (i.e. 7.6–20.3 cm diameter woody material). Other differences include the presence of live pine seedlings and fewer turkey oak as compared to other plots. This particular plot had the highest herbaceous and forb pre-fire loading and consumption with a higher fuel moisture content (205% as compared to next highest value of 144%). This high fuel moisture content was reflected in the ER for water, which was at least 4.7 times greater than the other plots (Table S3). The pyrolysis of cellulose (one of the three primary components of biomass as discussed below) forms levoglucosan. Shen et al. (2009) outline secondary decomposition pathways for levoglucosan, in which the initial step is the rehydration to generate glucopyranose. They demonstrate how glucopyranose can then form formaldehyde, methanol and acetic acid via secondary decomposition routes. This pathway (or a similar one) may have been favored at site 24B. The greater ERs for acetic acid and formaldehyde observed at 24B may have been influenced by the greater fraction of woody material and presence of herbaceous and forb fuels all with higher moisture contents. This hypothesis warrants further investigation.

Atmos. Chem. Phys. Discuss., https://doi.org/10.5194/acp-2019-174
Manuscript under review for journal Atmos. Chem. Phys.
Discussion started: 28 March 2019

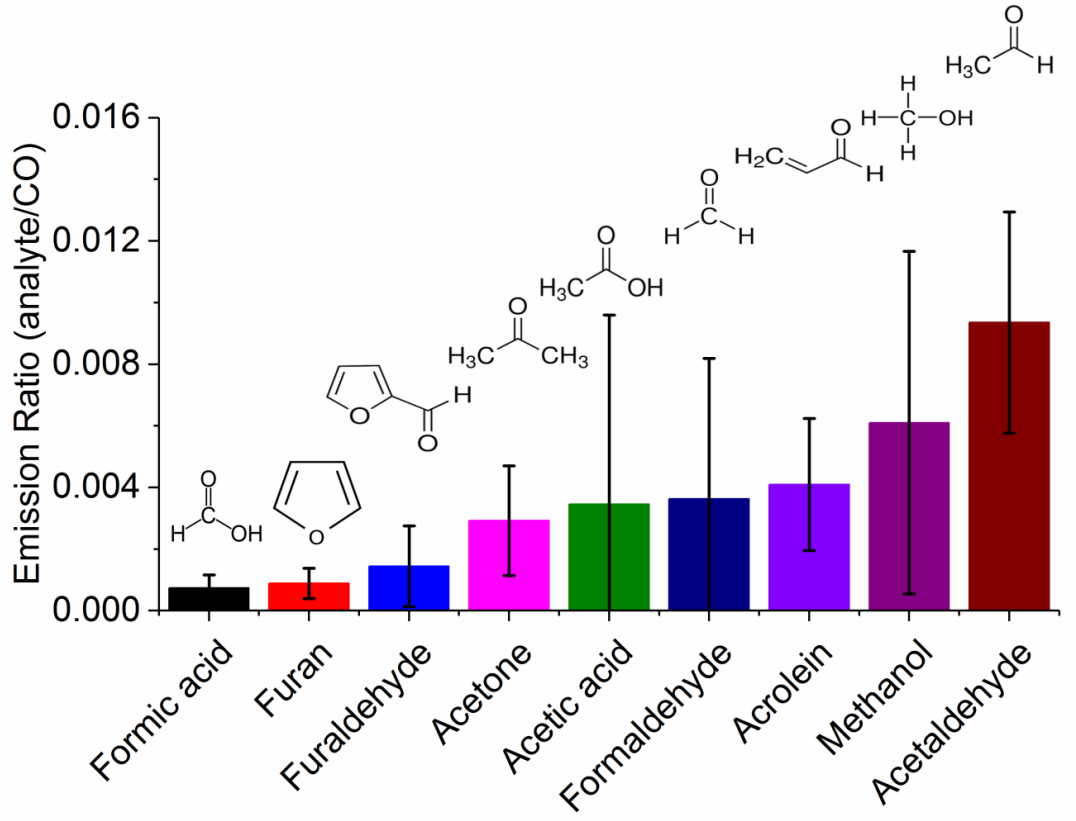

Figure 5. Average emission ratios (ppm/ppm$_{CO}$) for oxygenated hydrocarbons measured by FTIR for the 10 burn samples. Error bars represent 1σ.

Table 3 compares the present ER values with values from Akagi et al. (2013), Stockwell et al. (2014), Gilman et al. (2015) and Koss et al. (2018). The present ERs are comparable to other burn studies except for acetaldehyde, which appears to be marginally greater, and formaldehyde and acetic acid, which both appear to be lower. The higher ratio for acetaldehyde may be due to differences in the sampling approach as discussed above. That is, gas samples collected in the present study may contain species that were generated during an earlier period in the thermal decomposition process. In a controlled laboratory study by Stein et al (1983), acetaldehyde was observed as one of the initial products emitted from the pyrolysis of glycerol, a product pyrolyzed from levoglucosan. This same study also observed that acetaldehyde would continue to decompose

404 (under pyrolysis conditions) to smaller molecules such as ethene, methane, H_2 and CO (Stein et
405 al., 1983). The greater average ER for acetaldehyde observed in the present study may be due to
406 gases being captured (via the collection device) and removed from heat either in-between
407 decomposition steps or before combustion.

408

Table 3. Average emission ratios (ppb/ppm$_{CO}$) for this study and for previously published fire studies.

Analyte	This Study-Pine forest SC ground-based	Gilman et al., 2015 southeastern Fuels	Koss et al., 2018 study average for all fuels	Stockwell et al., 2014 Sawgrass SC	Stockwell et al., 2014 Ponderosa Pine MT	Akagi et al., 2013 Pine forest SC ground-based	Akagi et al., 2013 Pine forest SC air-based
Formic acid	0.7	1.6	2.2	0.7	5.1	n/a	0.6
Furan	0.9	0.7	1.9	0.8	1.2	2.4	1.1
Furaldehyde	1.5	1.5	2.1	n/a	n/a	0.1	0.2
Acetone	2.9	1.6	2.3	n/a	n/a	3.8	3.6
Formaldehyde	3.6	12	20	7.8	29	12	23
Acetic Acid	3.5	13	n/a	5.2	22	6.6	11
Acrolein	4.1	1.3	5.4	n/a	n/a	1.2	1.8
Methanol	6.1	7.8	12	3.4	24	21	13
Acetaldehyde	9.3	2.8	7.4	n/a	n/a	5.1	4.8

Koss et al. (2018) present the fire-integrated ERs. Gilman et al. (2015) present discrete ERs with sample acquisition of 20 to 300 sec. Stockwell et al. (2014) present the fire-integrated ERs. Akagi et al. (2013) present fire-averaged EFs calculated using ERs derived by the regression method. The emission ratios for Akagi et al. (2013) were obtained from the ratio of the emission factors for the analyte and CO multiplied by the molar mass of CO/molar mass of the analyte.

409

410 The slightly lower ERs for formaldehyde and acetic acid may in part be explained by secondary
411 decomposition pathways. Proposed pathways that generate formaldehyde and acetic acid proceed
412 through intermediates formed by the decomposition of levoglucosan (Shen and Gu, 2009).
413 Formaldehyde is generated from a number of intermediates such as hydroxyacetone (acetol)
414 (Lindenmaier et al., 2016) and 5-hydroxymethyl-furfural. While the formation mechanism for

415 acetic acid is via the decomposition of the intermediate hydroxyacetaldehyde (glycolaldehyde)
416 (Johnson et al., 2013), which undergoes a dehydration reaction to a ketene, and then a rehydration
417 to acetic acid (Shen and Gu, 2009), it is possible that the present conditions and fuels (save for site
418 24B) were not favorable for the above chemical pathways.

419 **3.5 Emissions of Aromatic Compounds**

420 In the present study, furan, furaldehyde and naphthalene were all detected via FTIR. Previous fire
421 studies have used FTIR to detect phenol and/or furan (Burling et al., 2011; Akagi et al., 2014;
422 Hatch et al., 2017; Christian et al., 2003; Christian et al., 2004; Stockwell et al., 2014; Karl et al.,
423 2007; Selimovic et al., 2018; Yokelson et al., 2013; Burling et al., 2010; Akagi et al., 2013). One
424 of these studies also detected furaldehyde (Selimovic et al., 2018). To the best of our knowledge,
425 however, this is the first burning study that has used IR spectroscopy to identify naphthalene vapor,
426 though it has previously been detected in biomass burning emissions via other methods (Koss et
427 al., 2018; Gilman et al., 2015). Naphthalene has also been detected in tar samples generated from
428 the controlled pyrolysis of similar fuels (Safdari et al., 2018).

429

430 Phenol and phenolic compounds were not definitively observed in this study due to their IR bands
431 being somewhat weak and obscured by a number of other species, namely acetic acid, carbon
432 dioxide, acetylene and hydrogen cyanide. However, phenolic compounds have been identified in
433 products generated from the pyrolysis of lignin in controlled laboratory experiments by Kibet et
434 al. (2012). Lignin, one of the three main components of biomass, can account for 10–35% of the
435 biomass, and its chemical structure consists of polymers of various phenolic alkyl side chain
436 subunits (Shen et al., 2015). When undergoing thermal decomposition, lignin will release volatiles
437 at temperatures between 200 and 400°C. The proposed mechanism can generate intermediates

438 such as phenoxy radicals that ultimately lead to the formation of phenols (Kibet et al., 2012). In
439 the present study, spectral evidence of phenol was in fact observed in some measurements, but the
440 IR bands at 1176 and 752 cm^{-1} were weak and were masked by other compound signatures,
441 hindering spectral quantification. Mixing ratios of phenol above the detection limit might have
442 been anticipated since prior controlled pyrolysis investigations of sparkleberry and longleaf pine
443 have detected phenol as a component in the tar (Safdari et al., 2018; Amini et al., 2019; Safdari et
444 al., 2019). While the phenol signal was weak, furan and furaldehyde, however, were clearly
445 detected, and their formation likely stemmed from thermal degradation of the other main
446 constituents of biomass. Besides lignin, the other primary macromolecular components are
447 cellulose and hemicellulose, which account for approximately 50% and 15–35% by weight,
448 respectively (Shen et al., 2015). The pyrolysis of cellulose is known to produce furaldehyde, furan
449 and other low weight oxygenated compounds (e.g. acetic acid) via the intermediate levoglucosan
450 (Bai et al., 2013). Moreover, furaldehyde and methanol have both been observed as volatile
451 products from the pyrolysis of methyl β-D-xylopyranoside, a model compound for xylan-based
452 hemicellulose (Shafizadeh et al., 1972).

453

454 Naphthalene is a polycyclic aromatic hydrocarbon (PAH) with several sources including a biomass
455 burning emission product. It was detected using FTIR for the first time in these studies (Scharko
456 et al., 2018). Its IR detection was not unexpected given that it has been observed in collected tar
457 samples generated by the laboratory pyrolysis of similar fuel types (Safdari et al., 2018) but its
458 identification in an experimental IR spectrum can be challenging as exemplified by Figure 6. Most
459 of its IR bands have only moderate cross-sections with the exception of the ν_{46} band, which has a
460 strong Q-branch at 782.3 cm^{-1} (green trace in Figure 6). For this band to be observed, however, it

Atmos. Chem. Phys. Discuss., https://doi.org/10.5194/acp-2019-174
Manuscript under review for journal Atmos. Chem. Phys.
Discussion started: 28 March 2019

461 needs to be deconvoluted from the acetylene rotational-vibrational lines also present in this spectral
462 domain (red trace in Figure 6). Better retrievals for naphthalene were obtained using a higher
463 spectral resolution (0.6 cm^{-1}) since the Q-branch of the ν_{46} band is quite sharp (FWHM ~ 1 cm^{-1}),
464 even at atmospheric pressure (Scharko et al., 2018).

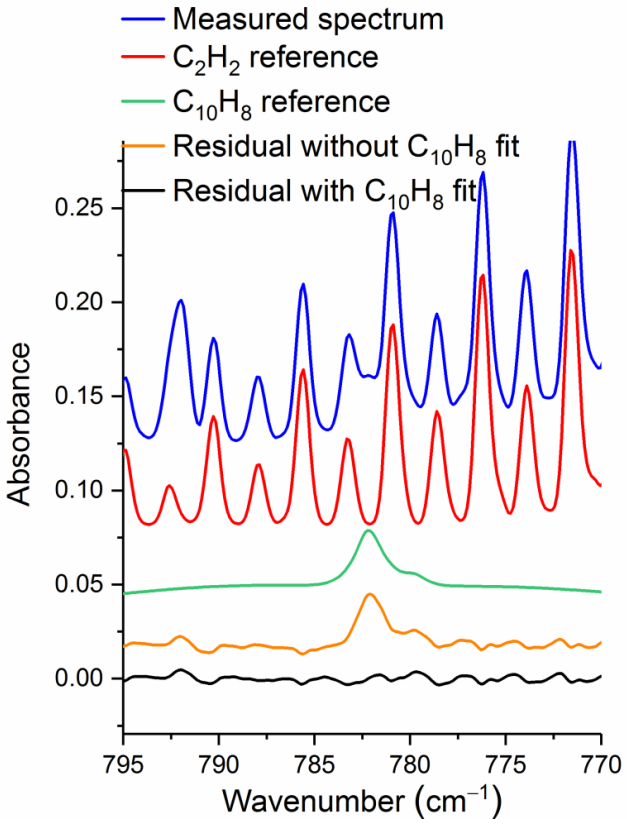

465

466 **Figure 6.** Measured and scaled reference spectra for acetylene (C_2H_2) and naphthalene ($C_{10}H_8$) as well as residual
467 with and without $C_{10}H_8$. The measurement is from site 16 plot 6 msmt. 2, and the detected mixing ratio for naphthalene
468 is 7.37 ppm. Spectra are offset for clarity. Reference absorption lines for acetylene are from HITRAN, and the
469 reference spectrum for naphthalene is from PNNL.

470

471 Figure 7a plots the mixing ratios (ppm) for naphthalene as a function of excess CO (ppm) while
472 Figure 7b displays the ERs for naphthalene for this study and previous studies.

Atmos. Chem. Phys. Discuss., https://doi.org/10.5194/acp-2019-174
Manuscript under review for journal Atmos. Chem. Phys.
Discussion started: 28 March 2019

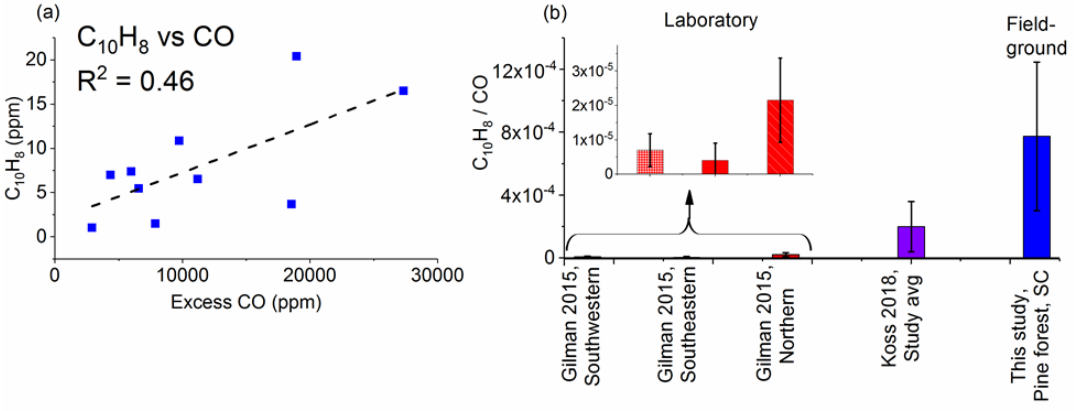

Figure 7. (a) Mixing ratios (ppm) for naphthalene ($C_{10}H_8$) as a function of excess CO (ppm) measured by FTIR for each of the 10 canisters. The dashed line is a linear fit. (b) Average emission ratios (ppm_{C10H8}/ppm_{CO}) for this study and for previous laboratory studies. Error bars represent 1σ. Koss et al. (2018) present the fire-integrated ERs. Gilman et al. (2015) present discrete ERs with sample acquisition of 20 to 300 sec.

The average naphthalene ER for this study is substantially greater than both the values from Gilman et al. (2015) and Koss et al. (2018). The average for Koss et al. (2018), however, is in turn an order of magnitude greater than the highest average for Gilman et al. (2015). The higher ER for naphthalene in this study (shown in Figure 7) clearly suggests that the method to capture pyrolysis gases was (at least in part) successful i.e. we were able to collect naphthalene gas prior to it having undergone secondary reactions. Besides oxidation, under the right conditions naphthalene can also continue to react forming still larger polyaromatics (Fairburn et al., 1990; Richter and Howard, 2000). Sekimoto et al., (2018) also linked naphthalene with the high temperature profile, and it appears that the samples in the present study were indeed collected when the high temperature process was dominant. The detection of naphthalene suggests that benzene and/or styrene, which are the main precursors to PAHs, may also be present. Styrene was not detected via FTIR methods, and benzene is challenging for IR analysis since its one strong band (ν_{11} mode at 673 cm^{-1}) is obfuscated by the CO_2 ν_2 bending mode under polluted atmospheric

conditions. Figure S3 shows the 50°C PNNL reference spectrum of benzene in the spectral regions where benzene's features are the strongest and experimental spectra (a) that are saturated and unusable in that region and (b) that are not saturated and used for identification.

3.6 Emissions of Nitrogen-containing Species

Gases such as NH_3, NO_2, NO, HCN and HONO have been identified using FTIR spectroscopy in fire laboratory experiments multiple times (Selimovic et al., 2018; Gilman et al., 2015; Christian et al., 2003; Christian et al., 2004; Goode et al., 1999; Yokelson et al., 1996; Yokelson et al., 1997; Stockwell et al., 2014; Hatch et al., 2017; Burling et al., 2010; Karl et al., 2007) as well as in field studies (Yokelson et al., 1999; Burling et al., 2011; Goode et al., 2000; Akagi et al., 2013; Karl et al., 2007; Akagi et al., 2014). Multiple other methods have also been used to detect N-containing gases, such as HNCO and CH_3CN (Gilman et al., 2015; Christian et al., 2003; Christian et al., 2004; Yokelson et al., 2009; Akagi et al., 2013; Karl et al., 2007; Roberts et al., 2010). The amount and speciation of N-containing compounds emitted is dependent on fuel type and nitrogen content (Stockwell et al., 2014; Burling et al., 2010; Coggon et al., 2016). Moreover, emissions can usually be linked to a stage of combustion: NO, NO_2, HNCO and HONO are all associated with the flaming stage, while NH_3 and HCN are primarily associated with smoldering combustion but have also been suggested as pyrolysis gases (Goode et al., 1999; Yokelson et al., 1996; Roberts et al., 2010; Burling et al., 2010; Hansson et al., 2004; Di Blasi, 2008). Biomass pyrolysis experiments carried out in an inert (i.e. oxygen free) atmosphere have revealed that NH_3, HCN and HNCO are all generated (Hansson et al., 2004). These compounds are all considered to be NO_x (NO + NO_2) and N_2O precursors because they are oxidized via combustion (Hansson et al., 2004).

514 The major N-containing compound identified in the present pyrolysis study was HCN. This is
515 consistent with previous small-scale and controlled laboratory studies that have shown HCN as
516 the primary N-product resulting from the pyrolysis of amino acids (Haidar et al., 1981; Johnson
517 and Kan, 1971). This observation is further evidence that the gas samples were extracted when
518 high temperature was the dominant process; Sekimoto et al., (2018) have associated HCN with the
519 high temperature pyrolysis profile. Figure 8a shows the correlation between HCN and excess CO
520 (R^2 = 0.89). Previous field fire studies have observed similar trends (Simpson et al., 2011;
521 Stockwell et al., 2016). Figure 8b shows a comparison between the ERs for HCN for this study as
522 well as from previous laboratory and field (both ground and airborne) studies. The present values
523 are comparable to other ground-based measurements (Guérette et al., 2018; Akagi et al., 2013) but
524 differ from a few of the laboratory and airborne-based studies. It should be noted that although
525 conducted at a different time of the year (late Oct./early Nov. 2011), the studies by Akagi et al.
526 (2013) took place near the same location as the current study (i.e. the same military base), and the
527 ERs for HCN between the studies are not significantly different for the ground-based
528 measurements. This suggests that the ratio of initial gases released of HCN to CO is consistent
529 with the ratio of these gases over the duration of the fire, or at least the fire-averaged ratio. With
530 regards to ERs for HCN, the major factor that appears to influence these values is fuel type,
531 particularly the fuel's peat content. Both laboratory (Stockwell et al., 2014) and field (Stockwell
532 et al., 2016) studies of Indonesian peat have shown greatly enhanced ERs for HCN compared to
533 the studies represented in Figure 8b, which consist mostly of pine, grasses and fuels of non-peat
534 origin. The range in the averages of ERs for HCN shown in Figure 8b is 0.0028–0.0095; the
535 averages for the Indonesian peat in laboratory and field studies were 0.015 and 0.021, respectively

536 (Stockwell et al., 2014; Stockwell et al., 2016), and are considerably higher than the range of values
537 seen in Figure 8b.

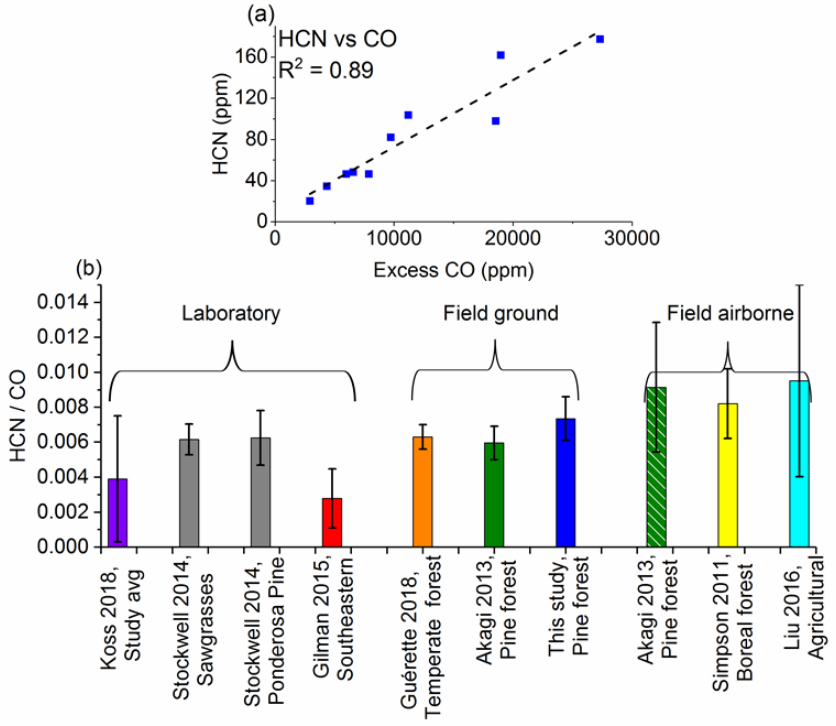

538
539 **Figure 8.** (a) Mixing ratios (ppm) for HCN as a function of excess CO (ppm) measured by FTIR. The dashed line is
540 a linear fit. (b) Average emission ratios (ppm/ppm CO) for this study and previous laboratory and field investigations.
541 Error bars represent 1σ. Koss et al. (2018) and Stockwell et al. (2014) present fire-integrated ERs. Gilman et al. (2015)
542 present discrete ERs with sample acquisition of 20–300 s. Simpson et al. (2011) present fire-averaged ERs derived by
543 regression. Guérette et al. (2018) present a single ER from all fires and derived by regression. Akagi et al. (2013) and
544 Liu et al. (2016) present fire-averaged EFs calculated using ERs derived by regression. The ERs for Akagi et al. (2013)
545 and Liu et al (2016) were derived from the ratio of the EFs for HCN and CO multiplied by the molar mass CO/molar
546 mass HCN.
547

548 In the present study, trace amounts of HONO were detected, but NH_3 was not observed. The
549 absence of NH_3 was somewhat unexpected since, similar to HCN, it is a known product from the
550 pyrolysis of amino acids (Haidar et al., 1981) and has been observed in prior prescribed fires
551 conducted at Ft. Jackson (Akagi et al., 2014; Akagi et al., 2013). There are several possible
552 explanations for the lack of NH_3 in the measurements. First, Sekimoto et al., (2018) observed that

553 NH_3 is associated more with a low temperature pyrolysis profile, and it appears that the present
554 samples were extracted during a period when high temperature pyrolysis was the main process.
555 Second, NH_3 is strongly linked with the smoldering phase (Goode et al., 1999; Yokelson et al.,
556 1996), and samples were not collected during this phase. Third, the speciation of the N-species
557 emitted is dependent on the fuel composition and amount of oxygen (Ren and Zhao, 2013a, b,
558 2012), so it is possible that in the present study, the conditions favored HCN instead of NH_3.
559 Fourth, experimentally NH_3 is known to adhere to certain surfaces (e.g. steel), and in this study it
560 may have adhered to the canisters or tubing walls and was thus not detected.

561

562 The IR quantification of other N-species, such as NO, NO_2, CH_3NO_2 and HNCO was obstructed
563 due to interferences from H_2O, CO and CO_2 as well as the low emission values for some of these
564 N-species. Since NO and NO_2 are usually associated with flaming combustion, it was not
565 unexpected that these species were not observed. HNCO has been linked with pyrolysis processes,
566 and its main formation pathway is the cracking of cyclic amides along with HCN which is also a
567 product of pyrolysis, Hansson et al. (2004).

568

569 After accounting for the challenges in measuring NO, NO_2 and HNCO, the second most prevalent
570 N-containing species observed in this work was methyl nitrite (CH_3ONO). Methyl nitrite has
571 previously been detected in emissions from biomass burning using other methods (Gilman et al.,
572 2015). Figure 9a shows the plot of mixing ratios for methyl nitrite as a function of excess CO.
573 Unlike HCN (Figure 8a), methyl nitrite exhibits minimal correlation with excess CO. As one
574 possible alternative explanation, methyl nitrite is known to be associated with rocket-propelled

grenades (RPGs), but the Ft. Jackson military base records did not indicate RPG usage in the burn plots (Scharko, 2019). While few fire studies have observed methyl nitrite, Gilman et al. (2015) have detected it using GC-MS. Figure 9b shows a comparison of the results from Gilman et al. (2015), separated by U.S. region, with the present results. It is worthy to note that both studies observed similar ERs and that in the Gilman study, methyl nitrite had the second highest mean ER after HCN for N-bearing species in southwestern fuels. Our observation of methyl nitrite is thus not unprecedented, but this was its first reported detection via FTIR (Scharko et al., 2018). In the present study, three measurements (Site 16, plot 1, msmt 1; Plot 24A, msmt 3; and Plot 24B) had higher ERs for methyl nitrite than the others (Figure S4a displays the individual ERs for each measurement), and it is unclear why this is the case. Other measurements collected at the same location reported lower ER values. If the three highest ER measurements in question are not included in the regression then the correlation between methyl nitrite and CO is stronger (Figure S4b), and the average ER is closer to values reported by Gilman et al. (2015) for southeastern fuels. One possible explanation for the three greater ER values is that the fuels may have contained more components such as nitrate esters and isopropyl nitrate, both of which are known to release minor amounts of methyl nitrite under controlled pyrolysis conditions (Boschan et al., 1955; Griffiths et al., 1975).

Atmos. Chem. Phys. Discuss., https://doi.org/10.5194/acp-2019-174
Manuscript under review for journal Atmos. Chem. Phys.
Discussion started: 28 March 2019

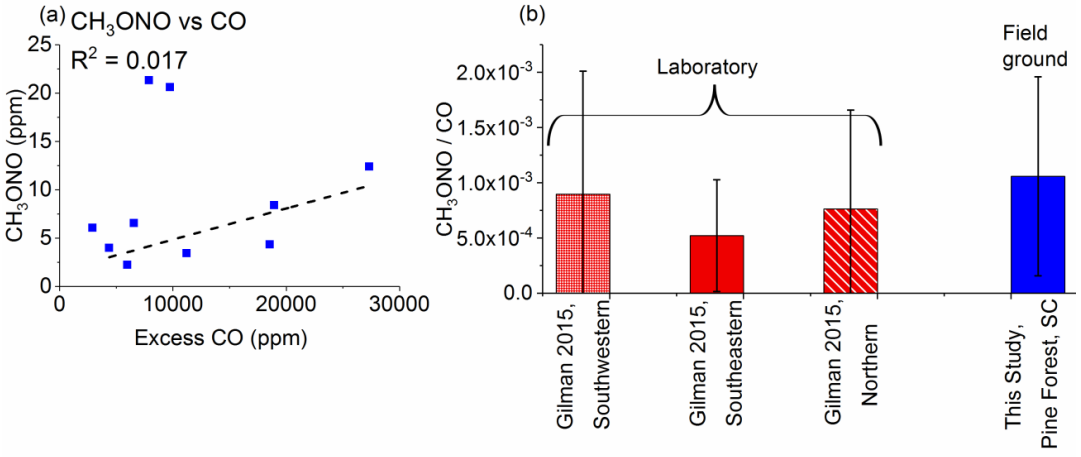

Figure 9. (a) Mixing ratios (ppm) for methyl nitrite (CH_3ONO) as a function of excess CO (ppm) as measured by FTIR. The dashed line is a linear fit. (b) Average emission ratios (ppm/ppm CO) for this study and previously published study carried out in the laboratory. Error bars represent 1σ. Gilman et al. (2015) present discrete ERs with sample acquisition of 20 to 300 s.

3.7 OH Reactivity

Most gases released from biomass burning will undergo secondary chemistry in the atmosphere. Other than photolysis or reactions with NO_3 or O_3, the primary destructive mechanism for most compounds is their oxidation by the OH radical (i.e. it governs the lifetimes of most components in the atmosphere). Along with the presence of VOCs and NO_x, the OH radical contributes to the formation of ozone and particulate matter (aerosols) (Atkinson, 2000; Finlayson-Pitts and Pitts Jr, 1999). In view of that, ozone and secondary organic aerosols have been measured in previous field biomass burning studies (Yokelson et al., 2009; Akagi et al., 2013). Additionally, prior fire studies have used OH reactivity as a metric to identify reactive species that may impact downwind chemistry (Gilman et al., 2015; Koss et al., 2018). OH reactivity has been defined as the loss frequency of OH due to its reaction with reactive species in the atmosphere and generally is expressed in units of s^{-1} (Zannoni et al., 2016). Here the quantity is relative to CO, and the units are s^{-1} ppm CO^{-1}. By multiplying the emission ratio by the associated OH rate constant, the

612 resulting quantity can provide an indication of which species are most likely to lead to ozone and
613 aerosol formation as a plume ages.

614

615 The OH reactivity was determined by the method outlined in Section 2.5 for each compound using
616 the ERs (Table S3) and previously reported OH rate constants (Table S6). The compounds were
617 grouped into four categories depending on their chemical structures. Alkanes, nitrogen containing
618 species and naphthalene were subsequently grouped together for clarity because their values were
619 low and not visible in Figure 10. The average total OH reactivity was 39.4 ± 9.8 s^{-1} ppm CO^{-1},
620 and the percent contributions per category are displayed in Figure 10a. The category with the
621 greatest percent contribution was alkenes with 75%. Figure 10b displays percent contribution for
622 each alkene to the total alkene OH reactivity. The specific alkene that had the greatest OH
623 reactivity was ethene with an average of 12.8 ± 2.0 s^{-1} ppm CO^{-1}, which was more than 1.8 times
624 the second highest value (propene with an average of 6.9 ± 1.7 s^{-1} ppm CO^{-1}). In a prior fire study,
625 Gilman et al. (2015) observed the largest contributions from propene (study average of 3.5 s^{-1} ppm
626 CO^{-1} using the same k_{OH} found in Table S6) and second largest with ethene (study average of 2.4
627 s^{-1} ppm CO^{-1} using the same k_{OH} found in Table S6). Although propene has a faster OH rate
628 constant than ethene, the high ERs observed for ethene in this study consequently enhanced its OH
629 reactivity above that of propene.

630

631 As previously discussed, the higher ERs for ethene (and other compounds, e.g. acetylene) are
632 likely due to high temperature pyrolysis being the dominant process with some pyrolytic gases
633 escaping the flame front. If that is indeed the case, the OH reactivities presented here reflect

634 emissions that have partly escaped some secondary pyrolysis and combustion reactions. Higher
635 ERs for acetylene were also observed; however, due to its relatively slow reaction with OH, its
636 average reactivity was 0.78 ± 0.2 s^{-1} ppm CO^{-1} (~2% of the total). Ethene, however, reacts faster
637 with OH. This OH-initiated reaction generates a hydroxyethyl radical, which propagates radicals
638 in the atmosphere through a series of reactions, leading to formation of both formaldehyde and
639 glycolaldehyde (Orlando et al., 1998).

640

641 The second category with the greatest fractional contribution was the oxygenated HCs, and the
642 major contributors were acetaldehyde and acrolein with reactivities of 3.7 ± 1.4 and 2.0 ± 1.4 s^{-1}
643 ppm CO^{-1}, respectively. Both of these aldehydes react with OH to form CO and formaldehyde as
644 well as peroxyacetylnitrate (PAN) for acetaldehyde (D'Anna et al., 2003) and
645 acryloylperoxynitrate (APAN) for acrolein (Orlando and Tyndall, 2002). Higher ERs for
646 acetaldehyde were observed. However, acrolein had a comparable average to the laboratory study
647 by Koss et al. (2018). The other two categories (furan and alkanes, nitrogen containing species
648 and naphthalene) had OH average reactivities of 2.1 ± 1.5 and 0.53 ± 0.3 s^{-1} ppm CO^{-1},
649 respectively. The individual OH reactivities for each measurement are displayed in Figure S5.
650 Consistent with the average, the category with the greatest fractional contribution was alkenes
651 followed by oxygenated HCs. Nonetheless, the measurement that had a significantly greater
652 contribution from the oxygenated HCs group (and less from alkenes) was site 24B. For site 24B,
653 the percent contribution of alkenes was 49% (study average = 75%) and for oxygenated HCs was
654 38% (study average = 18%).

Atmos. Chem. Phys. Discuss., https://doi.org/10.5194/acp-2019-174
Manuscript under review for journal Atmos. Chem. Phys.
Discussion started: 28 March 2019

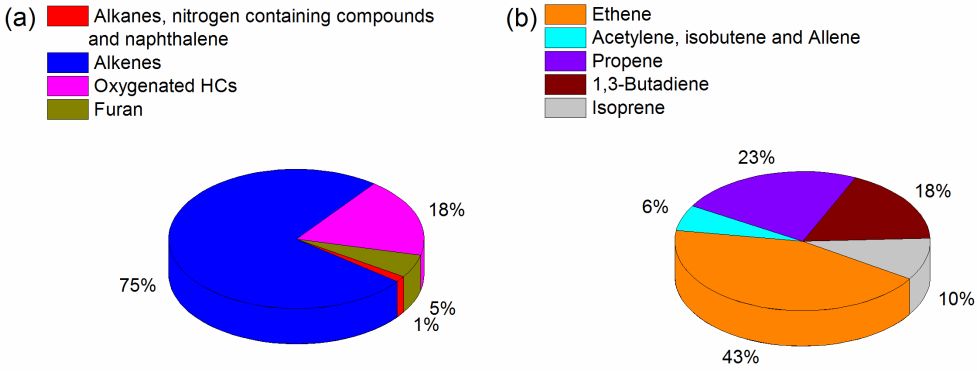

Figure 10. (a) Average percent contributions for the total OH reactivity for all ten measurements (39.4 ± 9.8 s^{-1} ppm CO^{-1}) and (b) the average percent contributions for each alkene to the total alkene OH reactivity (29.5 ± 8.7 s^{-1} ppm CO^{-1}). Error represents 1σ.

4. CONCLUSIONS

The objective of this study was to collect and quantify gas-phase compounds emitted ahead of the flame front (prior to the onset of combustion) in prescribed burns conducted in a pine forest. Primary and secondary decomposition pathways generate volatile products, which act as fuel gases that can undergo combustion and contribute to sustaining the fire. The main observations are that the estimated ratio of high to low temperature VOC emissions suggest that the samples were indeed extracted when the high temperature pyrolysis process was dominant. The acetylene/furan ratio suggested by Sekimoto (2018) was nearly 10x higher than previous studies; this is in fact consistent as previous works all had longer collection times, in some cases fire-averaged values. The significantly greater ERs observed for specific compounds, e.g. lightweight HCs such as ethene and acetylene as well as unoxidized aromatics such as naphthalene all support the hypothesis that the grab samples were collected prior to onset of decomposition, recombination or combustion reactions, and that such gases represent pyrolytic processes. For the oxidized organics,

674 acetaldehyde and methanol consistently had the highest ER values relative to CO for this collection
675 of pyrolysis gases. The ERs for acetic acid and formaldehyde were found to be high in some
676 instances, but this appeared to be related to fuel composition of the individual burn site. The major
677 N-component released was HCN, while NH_3 was not observed, which is consistent with the
678 collected gases representing species associated with the high temperature pyrolysis process.
679

680 ## ASSOCIATED CONTENT

681 ### Author contribution

682 NKS, TLM, and TJJ contributed to the writing of this manuscript. AMO and RGT set up laboratory
683 and recorded infrared data. NKS, AMO and CAB provided data processing and analysis. SPB,
684 ENL, JC, BMC and GMB aided in collection of field samples. JC provided thermal imaging and
685 videography. RDO and JRC contributed to fuel characterization. DRW and TJJ were the project
686 managers.

687 ### Supporting Information

688 The Supporting Information is available free of charge.

689 ## ACKNOWLEDGMENT

690 This work was supported by the Department of Defense's Strategic Environmental Research and
691 Development Program (SERDP), Project RC-2640 and we gratefully acknowledge our sponsor for
692 their support. PNNL is operated for the U.S. Department of Energy by the Battelle Memorial
693 Institute under contract DE-AC06-76RLO 1830. We gratefully thank David W. T. Griffith for his
694 valuable guidance and direction using the program MALT5 for spectral analysis. We are grateful
695 to John Maitland and colleagues at Fort Jackson for hosting the field campaign and carrying out

696 the burns. We thank Olivia Williams for help with spectral analysis using MALT5. In addition, we
697 are thankful to Professor Michael L. Myrick and his students at the University of South Carolina
698 for hosting us in their laboratory and for their helpful support setting up the instrument.

5. REFERENCES

NIST Chemical Kinetics Database: https://kinetics.nist.gov/kinetics/index.jsp, access: October 23, 2018.

Akagi, S. K., Yokelson, R. J., Wiedinmyer, C., Alvarado, M. J., Reid, J. S., Karl, T., Crounse, J. D., and Wennberg, P. O.: Emission factors for open and domestic biomass burning for use in atmospheric models, Atmos. Chem. Phys., 11, 4039-4072, 2011.

Akagi, S. K., Yokelson, R. J., Burling, I. R., Meinardi, S., Simpson, I., Blake, D. R., McMeeking, G. R., Sullivan, A., Lee, T., Kreidenweis, S., Urbanski, S., Reardon, J., Griffith, D. W. T., Johnson, T. J., and Weise, D. R.: Measurements of reactive trace gases and variable O_3 formation rates in some South Carolina biomass burning plumes, Atmos. Chem. Phys., 13, 1141-1165, 2013.

Akagi, S. K., Burling, I. R., Mendoza, A., Johnson, T. J., Cameron, M., Griffith, D. W. T., Paton-Walsh, C., Weise, D. R., Reardon, J., and Yokelson, R. J.: Field measurements of trace gases emitted by prescribed fires in southeastern US pine forests using an open-path FTIR system, Atmos. Chem. Phys., 14, 199-215, 2014.

Alves, C. A., Gonçalves, C., Pio, C. A., Mirante, F., Caseiro, A., Tarelho, L., Freitas, M. C., and Viegas, D. X.: Smoke emissions from biomass burning in a Mediterranean shrubland, Atmos. Environ., 44, 3024-3033, 2010.

Amini, E., Safdari, M.-S., DeYoung, J. T., Weise, D. R., and Fletcher, T. H.: Characterization of pyrolysis products from slow pyrolysis of live and dead vegetation native to the southern United States, Fuel, 235, 1475-1491, https://doi.org/10.1016/j.fuel.2018.08.112, 2019.

Andreae, M. O., Browell, E. V., Garstang, M., Gregory, G. L., Harriss, R. C., Hill, G. F., Jacob, D. J., Pereira, M. C., Sachse, G. W., Setzer, A. W., Silva Dias, P. L., Talbot, R. W., Torres, A. L., and Wofsy, S. C.: Biomass-burning emissions and associated haze layers over Amazonia, J. Geophys. Res. Atmos., 93, 1509-1527, 1988.

Andreae, M. O.: Biomass burning: Its history, use, and distribution and its impact on environmental quality and global climate, in: Global Biomass Burning: Atmospheric, Climatic, and Biospheric Implications, edited by: Levine, J. S., MIT Press, Cambridge, Mass, 3-21, 1991.

Andreae, M. O., Anderson, B. E., Blake, D. R., Bradshaw, J. D., Collins, J. E., Gregory, G. L., Sachse, G. W., and Shipham, M. C.: Influence of plumes from biomass burning on atmospheric chemistry over the equatorial and tropical South Atlantic during CITE 3, J. Geophys. Res. Atmos., 99, 12793-12808, 1994.

Andreae, M. O., and Merlet, P.: Emission of trace gases and aerosols from biomass burning, Global Biogeochem. Cycles, 15, 955-966, 2001.

Atkinson, R.: Atmospheric chemistry of VOCs and NO_x, Atmos. Environ., 34, 2063-2101, 2000.

Atkinson, R., and Arey, J.: Atmospheric degradation of volatile organic compounds, Chem. Rev., 103, 4605-4638, 2003.

Azeez, A. M., Meier, D., and Odermatt, J.: Temperature dependence of fast pyrolysis volatile products from European and African biomasses, J. Anal. Appl. Pyrolysis, 90, 81-92, 2011.

Bai, X., Johnston, P., Sadula, S., and Brown, R. C.: Role of levoglucosan physiochemistry in cellulose pyrolysis, J. Anal. Appl. Pyrolysis, 99, 58-65, 2013.

Boschan, R., Merrow, R. T., and van Dolah, R. W.: The chemistry of nitrate esters, Chem. Rev., 55, 485-510, 1955.

Burling, I. R., Yokelson, R. J., Griffith, D. W. T., Johnson, T. J., Veres, P., Roberts, J. M., Warneke, C., Urbanski, S. P., Reardon, J., Weise, D. R., Hao, W. M., and de Gouw, J.:

744 Laboratory measurements of trace gas emissions from biomass burning of fuel types from the
745 southeastern and southwestern United States, Atmos. Chem. Phys., 10, 11115-11130, 2010.
746 Burling, I. R., Yokelson, R. J., Akagi, S. K., Urbanski, S. P., Wold, C. E., Griffith, D. W. T.,
747 Johnson, T. J., Reardon, J., and Weise, D. R.: Airborne and ground-based measurements of the
748 trace gases and particles emitted by prescribed fires in the United States, Atmos. Chem. Phys.,
749 11, 12197-12216, 2011.
750 Cary, A.: Some relations of fire to longleaf pine, J. For., 30, 594-601, 1932.
751 Chi, C., Horn, D., Reznik, R., Zanders, D., Opferkuch, R., Nyers, J., Pierovich, J., Lavdas, L.,
752 Mcmahon, C., and Nelson, R.: Source assessment: prescribed burning, state of the art, US
753 Environmental Protection Agency, EPA (US) Report EPA-600/2-79-019h, 1979.
754 Christian, T. J., Kleiss, B., Yokelson, R. J., Holzinger, R., Crutzen, P. J., Hao, W. M., Saharjo, B.
755 H., and Ward, D. E.: Comprehensive laboratory measurements of biomass-burning emissions: 1.
756 Emissions from Indonesian, African, and other fuels, J. Geophys. Res. Atmos., 108, 4719,
757 10.1029/2003JD003704, 2003.
758 Christian, T. J., Kleiss, B., Yokelson, R. J., Holzinger, R., Crutzen, P. J., Hao, W. M., Shirai, T.,
759 and Blake, D. R.: Comprehensive laboratory measurements of biomass-burning emissions: 2.
760 First intercomparison of open-path FTIR, PTR-MS, and GC-MS/FID/ECD, J. Geophys. Res.
761 Atmos., 109, 2004.
762 Coggon, M. M., Veres, P. R., Yuan, B., Koss, A., Warneke, C., Gilman, J. B., Lerner, B. M.,
763 Peischl, J., Aikin, K. C., Stockwell, C. E., Hatch, L. E., Ryerson, T. B., Roberts, J. M., Yokelson,
764 R. J., and de Gouw, J. A.: Emissions of nitrogen-containing organic compounds from the burning
765 of herbaceous and arboraceous biomass: Fuel composition dependence and the variability of
766 commonly used nitrile tracers, Geophys. Res. Lett., 43, 9903-9912, 2016.
767 Collard, F.-X., and Blin, J.: A review on pyrolysis of biomass constituents: Mechanisms and
768 composition of the products obtained from the conversion of cellulose, hemicelluloses and
769 lignin, Renew. Sustainable Energy Rev., 38, 594-608, 2014.
770 Crutzen, P. J., Heidt, L. E., Krasnec, J. P., Pollock, W. H., and Seiler, W.: Biomass burning as a
771 source of atmospheric gases CO, H_2, N_2O, NO, CH_3Cl and COS, Nature, 282, 253-256,
772 10.1038/282253a0, 1979.
773 Crutzen, P. J., and Andreae, M. O.: Biomass burning in the tropics: Impact on atmospheric
774 chemistry and biogeochemical cycles, Science, 250, 1669-1678, 1990.
775 D'Anna, B., Bakken, V., Beukes, J. A., Nielsen, C. J., Brudnik, K., and Jodkowski, J. T.:
776 Experimental and theoretical studies of gas phase NO_3 and OH radical reactions with
777 formaldehyde, acetaldehyde and their isotopomers, Phys. Chem. Chem. Phys., 5, 1790-1805,
778 2003.
779 Di Blasi, C.: Modeling and simulation of combustion processes of charring and non-charring
780 solid fuels, Prog. Energy Combust. Sci., 19, 71-104, 1993.
781 Di Blasi, C.: Modeling chemical and physical processes of wood and biomass pyrolysis, Prog.
782 Energy Combust. Sci., 34, 47-90, 2008.
783 Dlugokencky, E., and Tans, P.: NOAA/ESRL www.esrl.noaa.gov/gmd/ccgg/trends/.
784 Fagernäs, L., Kuoppala, E., and Simell, P.: Polycyclic aromatic hydrocarbons in birch wood slow
785 pyrolysis products, Energy Fuels, 26, 6960-6970, 2012.
786 Fairburn, J. A., Behie, L. A., and Svrcek, W. Y.: Ultrapyrolysis of n-hexadecane in a novel
787 micro-reactor, Fuel, 69, 1537-1545, 1990.
788 Fernandes, P. M., and Botelho, H. S.: A review of prescribed burning effectiveness in fire hazard
789 reduction, Int. J. Wildland Fire, 12, 117-128, 2003.

790 Finlayson-Pitts, B. J., and Pitts Jr, J. N.: Chemistry of the upper and lower atmosphere: theory,
791 experiments, and applications, Elsevier, 1999.
792 Gilman, J. B., Lerner, B. M., Kuster, W. C., Goldan, P. D., Warneke, C., Veres, P. R., Roberts, J.
793 M., de Gouw, J. A., Burling, I. R., and Yokelson, R. J.: Biomass burning emissions and potential
794 air quality impacts of volatile organic compounds and other trace gases from fuels common in
795 the US, Atmos. Chem. Phys., 15, 13915-13938, 2015.
796 Goode, J. G., Yokelson, R. J., Susott, R. A., and Ward, D. E.: Trace gas emissions from
797 laboratory biomass fires measured by open-path Fourier transform infrared spectroscopy: Fires
798 in grass and surface fuels, J. Geophys. Res. Atmos., 104, 21237-21245, 1999.
799 Goode, J. G., Yokelson, R. J., Ward, D. E., Susott, R. A., Babbitt, R. E., Davies, M. A., and Hao,
800 W. M.: Measurements of excess O_3, CO_2, CO, CH_4, C_2H_4, C_2H_2, HCN, NO, NH_3, HCOOH,
801 CH_3COOH, HCHO, and CH_3OH in 1997 Alaskan biomass burning plumes by airborne Fourier
802 transform infrared spectroscopy (AFTIR), J. Geophys. Res. Atmos., 105, 22147-22166, 2000.
803 Gordon, I. E., Rothman, L. S., Hill, C., Kochanov, R. V., Tan, Y., Bernath, P. F., Birk, M.,
804 Boudon, V., Campargue, A., Chance, K. V., Drouin, B. J., Flaud, J.-M., Gamache, R. R.,
805 Hodges, J. T., Jacquemart, D., Perevalov, V. I., Perrin, A., Shine, K. P., Smith, M.-A. H.,
806 Tennyson, J., Toon, G. C., Tran, H., Tyuterev, V. G., Barbe, A., Császár, A. G., Devi, V. M.,
807 Furtenbacher, T., Harrison, J. J., Hartmann, J.-M., Jolly, A., Johnson, T. J., Karman, T., Kleiner,
808 I., Kyuberis, A. A., Loos, J., Lyulin, O. M., Massie, S. T., Mikhailenko, S. N., Moazzen-Ahmadi,
809 N., Müller, H. S. P., Naumenko, O. V., Nikitin, A. V., Polyansky, O. L., Rey, M., Rotger, M.,
810 Sharpe, S. W., Sung, K., Starikova, D., Tashkun, S. A., Vander Auwera, J., Wagner, G.,
811 Wilzewski, J., Wcisło, P., Yu, S., and Zak, E. J.: The HITRAN2016 molecular spectroscopic
812 database, J. Quant. Spectrosc. Radiat. Transfer, 203, 3-69, 2017.
813 Griffith, D. W. T.: MALT5 User guide Version 5.5.9, 2016.
814 Griffiths, J. F., Gilligan, M. F., and Gray, P.: Pyrolysis of isopropyl nitrate. I. Decomposition at
815 low temperatures and pressures, Combust. Flame, 24, 11-19, 1975.
816 Guérette, E.-A., Paton-Walsh, C., Desservettaz, M., Smith, T. E., Volkova, L., Weston, C. J., and
817 Meyer, C. P.: Emissions of trace gases from Australian temperate forest fires: emission factors
818 and dependence on modified combustion efficiency, Atmos. Chem. Phys., 18, 3717-3735, 2018.
819 Haidar, N. F., Patterson, J. M., Moors, M., and Smith Jr, W. T.: Effects of structure on pyrolysis
820 gases from amino acids, J. Agric. Food Chem., 29, 163-165, 1981.
821 Hansson, K.-M., Samuelsson, J., Tullin, C., and Åmand, L.-E.: Formation of HNCO, HCN, and
822 NH_3 from the pyrolysis of bark and nitrogen-containing model compounds, Combust. Flame,
823 137, 265-277, 2004.
824 Hatch, L. E., Yokelson, R. J., Stockwell, C. E., Veres, P. R., Simpson, I. J., Blake, D. R.,
825 Orlando, J. J., and Barsanti, K. C.: Multi-instrument comparison and compilation of non-
826 methane organic gas emissions from biomass burning and implications for smoke-derived
827 secondary organic aerosol precursors, Atmos. Chem. Phys., 17, 1471-1489, 2017.
828 Hurst, D. F., Griffith, D. W. T., Carras, J. N., Williams, D. J., and Fraser, P. J.: Measurements of
829 trace gases emitted by Australian savanna fires during the 1990 dry season, J. Atmos. Chem., 18,
830 33-56, 1994a.
831 Hurst, D. F., Griffith, D. W. T., and Cook, G. D.: Trace gas emissions from biomass burning in
832 tropical Australian savannas, J. Geophys. Res. Atmos. , 99, 16441-16456, 1994b.
833 Johnson, T. J., Profeta, L. T. M., Sams, R. L., Griffith, D. W. T., and Yokelson, R. L.: An
834 infrared spectral database for detection of gases emitted by biomass burning, Vib. Spectrosc., 53,
835 97-102, 2010.

836 Johnson, T. J., Sams, R. L., Profeta, L. T., Akagi, S. K., Burling, I. R., Yokelson, R. J., and
837 Williams, S. D.: Quantitative IR spectrum and vibrational assignments for glycolaldehyde vapor:
838 glycolaldehyde measurements in biomass burning plumes, J. Phys. Chem. A, 117, 4096-4107,
839 2013.
840 Johnson, W. R., and Kan, J. C.: Mechanisms of hydrogen cyanide formation from the pyrolysis
841 of amino acids and related compounds, J. Org. Chem., 36, 189-192, 1971.
842 Karl, T. G., Christian, T. J., Yokelson, R. J., Artaxo, P., Hao, W. M., and Guenther, A.: The
843 Tropical Forest and Fire Emissions Experiment: method evaluation of volatile organic compound
844 emissions measured by PTR-MS, FTIR, and GC from tropical biomass burning, Atmos. Chem.
845 Phys., 7, 5883-5897, 2007.
846 Kibet, J., Khachatryan, L., and Dellinger, B.: Molecular products and radicals from pyrolysis of
847 lignin, Environ. Sci. Technol., 46, 12994-13001, 2012.
848 Koss, A. R., Sekimoto, K., Gilman, J. B., Selimovic, V., Coggon, M. M., Zarzana, K. J., Yuan,
849 B., Lerner, B. M., Brown, S. S., Jimenez, J. L., Krechmer, J., Roberts, J. M., Warneke, C.,
850 Yokelson, R. J., and de Gouw, J.: Non-methane organic gas emissions from biomass burning:
851 identification, quantification, and emission factors from PTR-ToF during the FIREX 2016
852 laboratory experiment, Atmos. Chem. Phys., 18, 3299, 2018.
853 Ledesma, E. B., Marsh, N. D., Sandrowitz, A. K., and Wornat, M. J.: Global kinetic rate
854 parameters for the formation of polycyclic aromatic hydrocarbons from the pyrolyis of catechol,
855 a model compound representative of solid fuel moieties, Energy & fuels, 16, 1331-1336, 2002.
856 Lindenmaier, R., Tipton, N., Sams, R. L., Brauer, C. S., Blake, T. A., Williams, S. D., and
857 Johnson, T. J.: Assignment of the Fundamental Modes of Hydroxyacetone Using Gas-Phase
858 Infrared, Far-Infrared, Raman, and ab Initio Methods: Band Strengths for Atmospheric
859 Measurements, J. Phys. Chem. A, 120, 5993-6003, 2016.
860 Lindesay, J. A., Andreae, M. O., Goldammer, J. G., Harris, G., Annegarn, H. J., Garstang, M.,
861 Scholes, R. J., and Van Wilgen, B. W.: International geosphere-biosphere
862 programme/international global atmospheric chemistry SAFARI-92 field experiment:
863 Background and overview, J. Geophys. Res. Atmos., 101, 23521-23530, 1996.
864 Liu, X., Zhang, Y., Huey, L. G., Yokelson, R. J., Wang, Y., Jimenez, J. L., Campuzano-Jost, P.,
865 Beyersdorf, A. J., Blake, D. R., Choi, Y., St. Clair, H. M., Crounse, J. D., Day, D. A., Diskin, G.
866 S., Fried, A., Hall, S. R., Hanisco, T. F., King, L. E., Meinardi, S., Mikoviny, T., Palm, B. B.,
867 Peischl, J., Perring, A. E., Pollack, I. B., Ryerson, T. B., Sachse, G., Schwarz, J. P., Simpson, I.
868 J., Tanner, D. J., Thornhill, K. L., Ullmann, K., Weber, R. J., Wennberg, P. O., Wisthaler, A.,
869 Wolfe, G. M., and Ziemba, L. D.: Agricultural fires in the southeastern US during SEAC4RS:
870 Emissions of trace gases and particles and evolution of ozone, reactive nitrogen, and organic
871 aerosol, Journal of Geophysical Research: Atmospheres, 121, 7383-7414,
872 https://doi.org/10.1002/2016JD025040, 2016.
873 Lobert, J. M., Scharffe, D. H., Weimin, H., Kuhlbusch, T. A., Seuwen, R., Warneck, P., and
874 Crutzen, P. J.: Experimental evaluation of biomass burning emissions: Nitrogen and carbon
875 containing compounds, in: Global Biomass Burning. Atmospheric, climatic, and biospheric
876 implications, 1991.
877 Lu, Q., Yang, X.-c., Dong, C.-q., Zhang, Z.-f., Zhang, X.-m., and Zhu, X.-f.: Influence of
878 pyrolysis temperature and time on the cellulose fast pyrolysis products: Analytical Py-GC/MS
879 study, J. Anal. Appl. Pyrolysis, 92, 430-438, 2011.
880 Melvin, M. A.: National prescribed fire use survey report, Coalition of Prescribed Fire Councils
881 Technical Report, 01-12, 2012.

Miller, J. D., Safford, H. D., Crimmins, M., and Thode, A. E.: Quantitative evidence for increasing forest fire severity in the Sierra Nevada and southern Cascade Mountains, California and Nevada, USA, Ecosystems, 12, 16-32, 2009.

Orlando, J. J., Tyndall, G. S., Bilde, M., Ferronato, C., Wallington, T. J., Vereecken, L., and Peeters, J.: Laboratory and theoretical study of the oxy radicals in the OH-and Cl-initiated oxidation of ethene, J. Phys. Chem. A, 102, 8116-8123, 1998.

Orlando, J. J., and Tyndall, G. S.: Mechanisms for the reactions of OH with two unsaturated aldehydes: Crotonaldehyde and acrolein, J. Phys. Chem. A, 106, 12252-12259, 2002.

Palma, C. F.: Modelling of tar formation and evolution for biomass gasification: a review, Appl. Energy, 111, 129-141, 2013.

Paton-Walsh, C., Wilson, S. R., Jones, N. B., and Griffith, D. W. T.: Measurement of methanol emissions from Australian wildfires by ground-based solar Fourier transform spectroscopy, Geophys. Res. Lett., 35, 2008.

Paton-Walsh, C., Deutscher, N. M., Griffith, D. W. T., Forgan, B. W., Wilson, S. R., Jones, N. B., and Edwards, D. P.: Trace gas emissions from savanna fires in northern Australia, J. Geophys. Res. Atmos., 115, 2010.

Porcher, R. D., and Rayner, D. A.: A guide to the wildflowers of South Carolina, University of South Carolina Press Columbia, South Carolina, 2001.

Prichard, S., Ottmar, R., and Anderson, G.: Consume 3.0 user's guide. USDA Forest Service, p. 234, 2006.

Reid, J. S., Hyer, E. J., Prins, E. M., Westphal, D. L., Zhang, J., Wang, J., Christopher, S. A., Curtis, C. A., Schmidt, C. C., and Eleuterio, D. P.: Global monitoring and forecasting of biomass-burning smoke: Description of and lessons from the Fire Locating and Modeling of Burning Emissions (FLAMBE) program, IEEE J. Sel. Topics Appl. Earth Observ. Remote Sens., 2, 144-162, 2009.

Reinhardt, E. D., Keane, R. E., and Brown, J. K.: First order fire effects model: FOFEM 4.0, user's guide, Gen. Tech. Rep. INT-GTR-344. Ogden, UT: US Department of Agriculture, Forest Service, Intermountain Research Station. 65 p., 344, 1997.

Ren, Q., and Zhao, C.: NO_x and N_2O precursors from biomass pyrolysis: Nitrogen transformation from amino acid, Environ. Sci. Technol., 46, 4236-4240, 2012.

Ren, Q., and Zhao, C.: NO_x and N_2O precursors (NH_3 and HCN) from biomass pyrolysis: interaction between amino acid and mineral matter, Appl. Energy, 112, 170-174, 2013a.

Ren, Q., and Zhao, C.: NO_x and N_2O precursors from biomass pyrolysis: role of cellulose, hemicellulose and lignin, Environ. Sci. Technol., 47, 8955-8961, 2013b.

Richter, H., and Howard, J. B.: Formation of polycyclic aromatic hydrocarbons and their growth to soot—a review of chemical reaction pathways, Prog. Energy Combust. Sci., 26, 565-608, 2000.

Roberts, J. M., Veres, P., Warneke, C., Neuman, J. A., Washenfelder, R. A., Brown, S. S., Baasandorj, M., Burkholder, J. B., Burling, I. R., and Johnson, T. J.: Measurement of HONO, HNCO, and other inorganic acids by negative-ion proton-transfer chemical-ionization mass spectrometry (NI-PT-CIMS): Application to biomass burning emissions, Atmos. Meas. Tech., 3, 981, 2010.

Safdari, M.-S., Rahmati, M., Amini, E., Howarth, J. E., Berryhill, J. P., Dietenberger, M., Weise, D. R., and Fletcher, T. H.: Characterization of pyrolysis products from fast pyrolysis of live and dead vegetation native to the Southern United States, Fuel, 229, 151-166, 2018.

Safdari, M.-S., Amini, E., Weise, D. R., and Fletcher, T. H.: Heating rate and temperature effects on pyrolysis products from live wildland fuels, Fuel, 242, 295-304, 2019.
Sander, S. P., Golden, D. M., Kurylo, M. J., Moortgat, G. K., Wine, P. H., Ravishankara, A. R., Kolb, C. E., Molina, M. J., Finlayson-Pitts, B. J., Huie, R. E., and Orkin, V. L.: Chemical kinetics and photochemical data for use in atmospheric studies evaluation number 15, Pasadena, CA: Jet Propulsion Laboratory, National Aeronautics and Space Administration, 2006, 2006.
Scharko, N. K., Oeck, A. M., Tonkyn, R. G., Baker, S. P., Lincoln, E. N., Chong, J., Corcoran, B. M., Burke, G. M., Weise, D. R., Myers, T. L., Banach, C. A., and Johnson, T. J.: Identification of Gas-phase Pyrolysis Products in a Prescribed Fire: Seminal Detections Using Infrared Spectroscopy for Naphthalene, Methyl Nitrite, Allene, Acrolein and Acetaldehyde, Atmos. Meas. Tech. Discuss., 2018, 1-31, 10.5194/amt-2018-346, 2018.
Seinfeld, J. H., and Pandis, S. N.: Atmospheric chemistry and physics: from air pollution to climate change, John Wiley & Sons, 2012.
Selimovic, V., Yokelson, R. J., Warneke, C., Roberts, J. M., Gouw, J. d., Reardon, J., and Griffith, D. W. T.: Aerosol optical properties and trace gas emissions by PAX and OP-FTIR for laboratory-simulated western US wildfires during FIREX, Atmos. Chem. Phys., 18, 2929-2948, 2018.
Shafizadeh, F., McGinnis, G., and Philpot, C.: Thermal degradation of xylan and related model compounds, Carbohydr. Res., 25, 23-33, 1972.
Sharpe, S. W., Johnson, T. J., Sams, R. L., Chu, P. M., Rhoderick, G. C., and Johnson, P. A.: Gas-phase databases for quantitative infrared spectroscopy, Appl. Spectrosc., 58, 1452-1461, 2004.
Shen, D., Gu, S., and Bridgwater, A. V.: Study on the pyrolytic behaviour of xylan-based hemicellulose using TG–FTIR and Py–GC–FTIR, J. Anal. Appl. Pyrolysis, 87, 199-206, 2010.
Shen, D., Jin, W., Hu, J., Xiao, R., and Luo, K.: An overview on fast pyrolysis of the main constituents in lignocellulosic biomass to valued-added chemicals: Structures, pathways and interactions, Renew. Sustainable Energy Rev., 51, 761-774, 2015.
Shen, D. K., and Gu, S.: The mechanism for thermal decomposition of cellulose and its main products, Bioresour. Technol., 100, 6496-6504, https://doi.org/10.1016/j.biortech.2009.06.095, 2009.
Simmie, J. M.: Detailed chemical kinetic models for the combustion of hydrocarbon fuels, Prog. Energy Combust. Sci., 29, 599-634, 2003.
Simpson, I. J., Akagi, S. K., Barletta, B., Blake, N. J., Choi, Y., Diskin, G. S., Fried, A., Fuelberg, H. E., Meinardi, S., and Rowland, F. S.: Boreal forest fire emissions in fresh Canadian smoke plumes: C_1-C_{10} volatile organic compounds (VOCs), CO_2, CO, NO_2, NO, HCN and CH_3CN, Atmos. Chem. Phys., 11, 6445-6463, 2011.
Stein, Y. S., Antal Jr, M. J., and Jones jr, M.: A study of the gas-phase pyrolysis of glycerol, J. Anal. Appl. Pyrolysis, 4, 283-296, 1983.
Stockwell, C. E., Yokelson, R., Kreidenweis, S. M., Robinson, A. L., DeMott, P. J., Sullivan, R. C., Reardon, J., Ryan, K. C., Griffith, D. W. T., and Stevens, L.: Trace gas emissions from combustion of peat, crop residue, domestic biofuels, grasses, and other fuels: configuration and Fourier transform infrared (FTIR) component of the fourth Fire Lab at Missoula Experiment (FLAME-4), Atmos. Chem. Phys., 14, 9727-9754, 2014.
Stockwell, C. E., Jayarathne, T., Cochrane, M. A., Ryan, K. C., Putra, E. I., Saharjo, B. H., Nurhayati, A. D., Albar, I., Blake, D. R., Simpson, I. J., Stone, E. A., and Yokelson, R. J.: Field

measurements of trace gases and aerosols emitted by peat fires in Central Kalimantan, Indonesia, during the 2015 El Niño, Atmos. Chem. Phys., 16, 11711-11732, 2016.
Talbot, R. W., Beecher, K. M., Harriss, R. C., and Cofer, W. R.: Atmospheric geochemistry of formic and acetic acids at a mid-latitude temperate site, J. Geophys. Res. Atmos., 93, 1638-1652, 1988.
Turetsky, M. R., Kane, E. S., Harden, J. W., Ottmar, R. D., Manies, K. L., Hoy, E., and Kasischke, E. S.: Recent acceleration of biomass burning and carbon losses in Alaskan forests and peatlands, Nat. Geosci., 4, 27, https://doi.org/10.1038/NGEO1027, 2011.
Urbanski, S. P.: Combustion efficiency and emission factors for wildfire-season fires in mixed conifer forests of the northern Rocky Mountains, US, Atmos. Chem. Phys., 13, 7241-7262, 2013.
Waldrop, T. A., and Goodrick, S. L.: Introduction to prescribed fires in Southern ecosystems, Science Update SRS-054. Asheville, NC: US Department of Agriculture Forest Service, Southern Research Station. 80 p., 54, 1-80, 2012.
Ward, D., Susott, R., Kauffman, J., Babbitt, R., Cummings, D., Dias, B., Holben, B., Kaufman, Y., Rasmussen, R., and Setzer, A.: Smoke and fire characteristics for cerrado and deforestation burns in Brazil: BASE-B experiment, J. Geophys. Res. Atmos. , 97, 14601-14619, 1992.
Ward, D. E., and Hao, W.: Projections of emissions from burning of biomass for use in studies of global climate and atmospheric chemistry, Paper 91-128.4. Presented at the 84th Annual Meeting and Exhibition; Vancouver, British Columbia; June 16-21, 1991. Air and Waste Management Association. 16 p., 1991,
Ward, D. E., and Hardy, C. C.: Smoke emissions from wildland fires, Environ. Int., 17, 117-134, 1991.
Ward, D. E., Hao, W. M., Susott, R. A., Babbitt, R. E., Shea, R. W., Kauffman, J. B., and Justice, C. O.: Effect of fuel composition on combustion efficiency and emission factors for African savanna ecosystems, J. Geophys. Res. Atmos., 101, 23569-23576, 1996.
Wooster, M. J., Freeborn, P. H., Archibald, S., Oppenheimer, C., Roberts, G. J., Smith, T. E. L., Govender, N., Burton, M., and Palumbo, I.: Field determination of biomass burning emission ratios and factors via open-path FTIR spectroscopy and fire radiative power assessment: headfire, backfire and residual smouldering combustion in African savannahs, Atmos. Chem. Phys., 11, 11591-11615, 2011.
Yokelson, R. J., Griffith, D. W. T., and Ward, D. E.: Open-path Fourier transform infrared studies of large-scale laboratory biomass fires, J. Geophys. Res. Atmos., 101, 21067-21080, 1996.
Yokelson, R. J., Susott, R., Ward, D. E., Reardon, J., and Griffith, D. W. T.: Emissions from smoldering combustion of biomass measured by open-path Fourier transform infrared spectroscopy, J. Geophys. Res. Atmos., 102, 18865-18877, 1997.
Yokelson, R. J., Goode, J. G., Ward, D. E., Susott, R. A., Babbitt, R. E., Wade, D. D., Bertschi, I., Griffith, D. W. T., and Hao, W. M.: Emissions of formaldehyde, acetic acid, methanol, and other trace gases from biomass fires in North Carolina measured by airborne Fourier transform infrared spectroscopy, J. Geophys. Res. Atmos., 104, 30109-30125, 1999.
Yokelson, R. J., Crounse, J. D., DeCarlo, P. F., Karl, T., Urbanski, S. P., Atlas, E., Campos, T., Shinozuka, Y., Kasputin, V., Clarke, A. D., Weinheimer, A., Knapp, D. J., Montzka, D. D., Holloway, J., Weibring, P., Flocke, F., Zheng, W., Toohey, D., Wennberg, P. O., Wiedinmyer, C., Mauldin, L., Fried, A., Richter, D., Walega, J., Jimenez, J. L., Adachi, K., Buseck, P. R., Hall, S. R., and Shetter, R.: Emissions from biomass burning in the Yucatan, Atmos. Chem. Phys., 9, 5785, 2009.

1018 Yokelson, R. J., Burling, I. R., Gilman, J. B., Warneke, C., Stockwell, C. E., Gouw, J. d., Akagi,
1019 S. K., Urbanski, S. P., Veres, P., Roberts, J. M., Kuster, W. C., Reardon, J., Griffith, D. W. T.,
1020 Johnson, T. J., Hosseini, S., Miller, J. W., Cocker III, D. R., Jung, H., and Weise, D. R.:
1021 Coupling field and laboratory measurements to estimate the emission factors of identified and
1022 unidentified trace gases for prescribed fires, Atmos. Chem. Phys., 13, 89-116, 2013.
1023 Young, V. L., Kieser, B. N., Chen, S. P., and Niki, H.: Seasonal trends and local influences on
1024 nonmethane hydrocarbon concentrations in the Canadian boreal forest, J. Geophys. Res. Atmos.,
1025 102, 5913-5918, 1997.
1026 Zannoni, N., Gros, V., Lanza, M., Sarda, R., Bonsang, B., Kalogridis, C., Preunkert, S., Legrand,
1027 M., Jambert, C., Boissard, C., and Lathiere, J.: OH reactivity and concentrations of biogenic
1028 volatile organic compounds in a Mediterranean forest of downy oak trees, Atmos. Chem. Phys.,
1029 16, 1619-1636, 2016.

1030